

Models for Stilbene Photoisomerization: Experimental and Theoretical Studies of the Excited-State Dynamics of 1,2-Diphenylcycloalkenes

John H. Frederick,*

Department of Chemistry, University of Nevada, Reno, Nevada 89557

Y. Fujiwara,

School of Pharmaceutical Sciences, Kanazawa University, Kanazawa 920, Japan

John H. Penn,

Department of Chemistry, University of West Virginia, Morgantown, West Virginia 26506-6045

Keitaro Yoshihara,* and Hrvoje Petek*

Institute for Molecular Science, Myodaiji, Okazaki 444, Japan (Received: October 3, 1990)

The initial dynamics in the photoisomerization of *cis*-stilbene, especially the dynamics leading to photocyclization, is explored by studying the high-resolution spectroscopy and implied dynamics of a series of 1,2-diphenylcycloalkenes. These molecules are isochromophoric to *cis*-stilbene but are structurally hindered from undergoing *cis*-*trans* isomerization. In particular, the high-resolution fluorescence excitation spectrum of 1,2-diphenylcyclobutene (DPC-4) reveals detailed information about the symmetric in-plane bend and symmetric phenyl ring twist motions, which are crucial to photocyclization. The DPC-4 spectrum is analyzed theoretically, and an empirical surface is constructed for the S_1 state that reproduces both line positions and relative intensities in the observed spectrum. An extrapolation of the DPC-4 potential surface is then made to construct S_1 state surfaces for 1,2-diphenylcyclopentene (DPC-5), 1,2-diphenylcyclohexene (DPC-6), and *cis*-stilbene. These surfaces all indicate that the initial dynamics of the molecule is to smaller bend angles and smaller phenyl twist angles upon excitation to the excited singlet state. Evidence for the importance of photocyclization in the dynamics of excited state *cis*-stilbene is presented and discussed.

I. Introduction

Detailed understanding of the isomerization dynamics of *cis*-stilbene requires knowledge about the shape of the potential energy surface on which the isomerization dynamics occurs. The measured ~ 1.3 -ps lifetime of the *cis*-stilbene S_1 state in room-temperature solution¹⁻³ and the deduced 7:3 branching ratio for the decay through *cis*-*trans* and conrotatory photocyclization isomerization channels⁴ suggest that the dynamics are determined by the shape of the potential energy surface, which governs the initial vibrational motion of the nuclei upon excitation to the S_1 surface. The motivation for studying in detail the isomerization dynamics of model systems such as *cis*-stilbene is to provide a basis for understanding more complex biologically important processes such as the role of *cis*-*trans* isomerization in vision,⁵ as well as technologically important photochromic photocyclization reaction of *cis*-stilbene-like systems.^{6,7} Unfortunately, the *cis*-stilbene $S_1 \leftarrow S_0$ absorption spectrum, which is $<5000\text{ cm}^{-1}$ broad and structureless and whose maximum is displaced by $<6000\text{ cm}^{-1}$ from the origin,⁸ does not provide much information from which the shape of the excited-state surface could be deduced. The *ab initio* theoretical calculation of the *cis*-stilbene excited-state surface is an unanswered challenge for quantum chemists. Since it is difficult to extract structural information on *cis*-stilbene directly from its absorption spectrum, several groups have taken more indirect approaches, but at present there is no coherent model that can fully explain the *cis*-stilbene photophysics and photochemistry.

The current understanding of the *cis*-stilbene S_1 state surface has been derived from (i) high-resolution spectroscopy of the *trans*-stilbene S_1 state;⁹⁻¹³ (ii) semiempirical calculations;^{14,15} (iii) measurements of photochemical products from both *cis*- and *trans*-stilbene over a wide range in temperature and solvent viscosity;¹⁶⁻¹⁹ (iv) transient absorption² and emission³ spectroscopy upon excitation of the *cis*-stilbene S_1 state; (v) resonance Raman spectroscopy of *cis*-stilbene;²⁰ (vi) the vibrationally resolved spectroscopy of 1,2-diphenylcyclobutene (DPC-4) and dibenzosuberene

and reaction dynamics of other 1,2-diphenylcycloalkenes.⁴ Much of this work has been described in the recent review by Waldeck.¹ Our understanding of the *cis*-stilbene electronic surfaces in coordinates that are relevant to the isomerization dynamics is summarized in Figure 1 and described in greater detail in the next section.

- (1) Waldeck, D. H. *Chem. Rev.*, in press.
- (2) Abrash, S.; Repinec, S.; Hochstrasser, R. M. *J. Chem. Phys.* **1990**, *93*, 1041.
- (3) Todd, D. C.; Jean, J. M.; Rosenthal, S. J.; Ruggiero, A. J.; Yang, D.; Fleming, G. R. *J. Chem. Phys.* **1990**, *93*, 8658.
- (4) Petek, H.; Yoshihara, K.; Fujiwara, Y.; Lin, Z.; Penn, J. H.; Frederick, J. H. *J. Phys. Chem.* **1990**, *94*, 7539.
- (5) Yoshizawa, T.; Kandori, H. *Progress in Retinal Research*; Osborne, N. N., Chader, G. J., Eds.; Pergamon Press: Oxford; Vol. 11, in press.
- (6) Muszkat, K. A. *Top. Curr. Chem.* **1980**, *88*, 89.
- (7) Mallory, F. B.; Mallory, C. W. *Organic Reactions*; Wiley: New York, 1983; Vol. 30.
- (8) Dyck, R. H.; McClure, D. S. *J. Chem. Phys.* **1962**, *36*, 2326.
- (9) Champagne, B. B.; Pfanstiel, J. F.; Plusquellic, D. F.; Pratt, D. W.; van Herpen, W. M.; Meerts, W. L. *J. Phys. Chem.* **1990**, *94*, 6.
- (10) Syage, J. A.; Felker, P. M.; Zewail, A. H. *J. Chem. Phys.* **1984**, *81*, 4685.
- (11) Suzuki, T.; Mikami, N.; Ito, M. *J. Phys. Chem.* **1986**, *90*, 6431.
- (12) Spangler, L. H.; van Zee, R.; Zwier, T. S. *J. Phys. Chem.* **1987**, *91*, 2782.
- (13) Urano, T.; Hamaguchi, H.; Tasumi, M.; Yamanouchi, K.; Tsuchiya, K.; Gustafson, T. L. *J. Chem. Phys.* **1989**, *91*, 3884.
- (14) Muszkat, K. A.; Schmidt, W. *Helv. Chim. Acta* **1971**, *54*, 1195.
- (15) Warshel, A. *J. Chem. Phys.* **1975**, *62*, 214.
- (16) Muszkat, K. A.; Fischer, E. *J. Chem. Soc. B* **1967**, 663. Wismonski-Knittel, T.; Fischer, G.; Fischer, E. *J. Chem. Soc., Perkin Trans. I* **1974**, 1930.
- (17) Malkin, S.; Fischer, E. *J. Phys. Chem.* **1964**, *68*, 1153. Gegiou, D.; Muszkat, K. A.; Fischer, E. *J. Am. Chem. Soc.* **1968**, *90*, 3907. Gegiou, D.; Muszkat, K. A.; Fischer, E. *J. Am. Chem. Soc.* **1968**, *90*, 12.
- (18) Sharafy, S.; Muszkat, K. A. *J. Am. Chem. Soc.* **1971**, *93*, 4119.
- (19) Saltiel, J.; Marinari, A.; Chang, D. W. L.; Mitchener, J. C.; Megarity, E. D. *J. Am. Chem. Soc.* **1979**, *101*, 2982.
- (20) Myers, A. B.; Mathies, R. A. *J. Chem. Phys.* **1984**, *81*, 1552.

* To whom correspondence should be addressed.

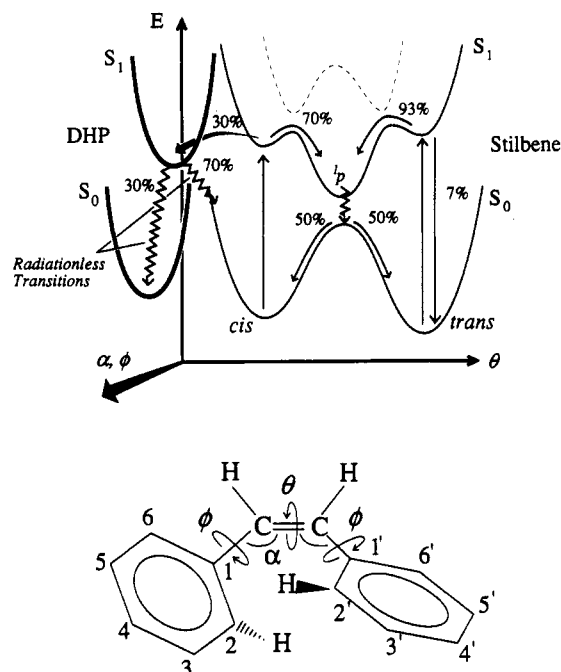


Figure 1. Schematic potential energy surfaces of *cis*-stilbene in α , ϕ , and θ coordinates, which are involved in the *cis*-*trans* and photocyclization isomerization reactions. These angles are schematically portrayed below the potential energy surfaces. The barrier to DHP formation on the S_1 of 1.2 kcal/mol was determined in ref 16. According to the calculations of Muszkat and Schmidt, the isomerization occurs on a single adiabatic surface.¹⁴ The existence of a low barrier (<1 kcal/mol) for the *cis*-*trans* isomerization is more tenuous, because it is difficult to separate the intrinsic barrier from the viscosity effects of comparable magnitude. This barrier is thought to be a result of the crossing between 1B_u and a higher energy 1A_g surface.

Since *trans*-stilbene is strongly fluorescent at low temperatures, such as in a supersonic beam, numerous workers have studied its structure in the S_1 state using vibrationally resolved spectroscopy,¹⁰⁻¹³ and recently, Pratt and co-workers⁹ have succeeded in measuring and analyzing ultrahigh-resolution rotationally resolved laser-induced fluorescence (LIF) spectrum of the S_1 state. The analyses of the vibrational and rotational spectra show that upon excitation to the S_1 state of *trans*-stilbene (i) the $C_6=C_7$ bond order decreases and the bond length increases, (ii) the C_6-C_1 bond order increases and the bond length decreases, (iii) the $C_6=C_7-C_1$ bond angle decreases, and (iv) the force constant for phenyl ring twisting about ϕ increases.

Although the differences between S_0 and S_1 structures in *trans*-stilbene are minor, the barrier for *cis*-*trans* isomerization in the S_1 state is much lower (<1200 cm^{-1} for the isolated molecule).^{10,21} Such a low barrier is thought to be the outcome of a crossing between the 1B_u symmetry S_1 state and a higher energy 1A_g symmetry state. Crossing over this barrier along the θ coordinate to a 90° twisted configuration, the postulated "phantom state",^{22a} leads to production of *cis*-stilbene with nearly 50% quantum yield at room temperature.¹⁷⁻¹⁹ We note that the exact mechanism of *cis*-*trans* isomerization and the existence and nature of the phantom state remain unresolved.^{2,22b}

Since the π -electronic structure of *cis*-stilbene is similar to that of *trans*-stilbene (at least in the planar configuration), it may be argued that similar electronic-state coupling as in *trans*-stilbene will result in a low barrier to isomerization. The absence of fluorescence from *cis*-stilbene except in low-temperature high-viscosity organic solvent glasses^{17,18} has been used as evidence against such a barrier. However, recent measurements of long-

lived (17.2 ns) emission from *cis*-stilbene in Ar and Kr clusters has been interpreted as evidence for a shallow minimum.^{23,24} Since the phenyl ring steric interactions distort *cis*-stilbene from the planar configuration, this minimum appears to be significantly shallower than for *trans*-stilbene.

Although the present understanding of *trans*-stilbene structure is a useful basis for understanding some aspects of the *cis*-stilbene structure and dynamics, the differences between the electronic spectra and dynamics of the two isomers are striking. These differences can be traced to the interactions between phenyl rings in *cis*-stilbene, which are dominated by C_2-C_2' and H_2-H_2' repulsive interactions in the ground state and C_2-C_2' attractive and H_2-H_2' repulsive interactions in the first excited state.^{4,25} Because of the difference in these interactions *cis*-stilbene undergoes drastic changes in the angles α , ϕ , θ upon excitation to the S_1 state, which partly explains the large displacement of the absorption maximum from the origin and the large red shift of the emission maximum.^{4,15} The phenyl ring interaction also affects the *cis*-stilbene isomerization dynamics. In regions of the potential surface where the H_2-H_2' repulsion dominates, the *cis*-*trans* isomerization process is more favored; whereas, in regions where the H_2-H_2' repulsion is weak and the C_2-C_2' attraction is strong, a new isomerization channel involving the conrotatory photocyclization to dihydrophenanthrene becomes available with a small barrier of $\sim 420 \text{ cm}^{-1}$ (1.2 kcal/mol).^{4,16} The C_2-C_2' interaction exerts an additional effect on the spectrum because it mixes configurations of dodecahexaene-like excited electronic state with the stilbene S_1 state.

The application of several different experimental techniques to the determination of the *cis*-stilbene structure has led to conflicting conclusions. The most direct method available for determining the structure of molecules with diffuse absorption spectra is resonance Raman spectroscopy, which has been applied by Myers and Mathies.²⁰ They have interpreted the resonance Raman spectrum of *cis*-stilbene using Heller's wave packet formalism²⁶ and come to the conclusion that the initial motion on *cis*-stilbene S_1 surface is along a repulsive ethylenic torsion coordinate, leading to 35° torsion 20 fs after the excitation. Although it is plausible that a significant change in the angle θ can occur on this time scale, this initial rearrangement should not be identified with isomerization, because *cis*-*trans* isomerization occurs on a ~ 1 -ps time scale.

Recently, the groups of Hochstrasser² and Fleming³ have studied the nonradiative decay of *cis*-stilbene using transient absorption and gated fluorescence techniques. The time scale of these experiments (100–200 fs) was sufficient to measure the S_1 state decay but not to observe any significant time evolution of the absorption or emission spectra. If the *cis*-*trans* isomerization process were a simple torsion about the $C_6=C_7$ bond on a purely repulsive potential, there should be significant time evolution of the excited-state absorption and emission spectra on a ~ 1 -ps time scale. Apparently, the time evolution occurs on less than a 100-fs time scale and therefore probably involves large displacements along high-frequency modes such as $C=C$ and $C-C$ stretches, which would be consistent with large changes in conjugation in the S_1 state.

Although Hochstrasser's and Fleming's groups measured very similar nonradiative decay rates of *cis*-stilbene, their interpretation of the viscosity effects led them to slightly different conclusions. Hochstrasser et al. reasoned that the observed exponential decays and lack of spectral evolution support the existence of a small minimum on the S_1 surface.² Although Fleming and co-workers could not explain their measurements using the Bagchi-Flem-

(23) Petek, H.; Fujiwara, Y.; Kim, D.; Yoshihara, K. *J. Am. Chem. Soc.* **1988**, *110*, 6269.

(24) Petek, H.; Yoshihara, K.; Fujiwara, Y.; Frey, J. G. *J. Opt. Soc. Am. B* **1990**, *7*, 1540. Petek, H.; Yoshihara, K.; Fujiwara, Y.; Frey, J. G. *Ultrafast Phenomena*; Springer: New York, Vol. VII, in press.

(25) Hohlneicher, G.; Müller, M.; Demmer, M.; Lex, J.; Penn, J. H.; Gan, L. X.; Loesel, P. D. *J. Am. Chem. Soc.* **1988**, *110*, 4483.

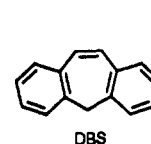
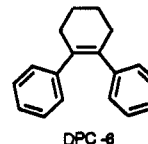
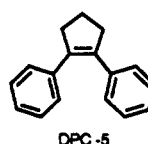
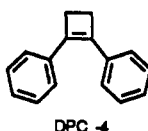
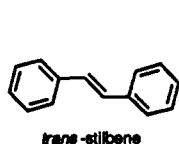
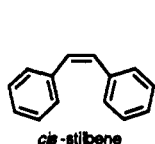
(26) Lee, S. Y.; Heller, E. J. *J. Chem. Phys.* **1979**, *71*, 4777. Heller, E. J.; Sundberg, R. L.; Tannor, D. *J. Phys. Chem.* **1982**, *86*, 1822.

(21) Courtney, S. H.; Balk, M. W.; Phillips, L. A.; Webb, S. P.; Yang, D.; Levy, D. H.; Fleming, G. R. *J. Chem. Phys.* **1988**, *89*, 6697. Amirav, A.; Jortner, J. *Chem. Phys. Lett.* **1983**, *95*, 295.

(22) (a) Saitiel, J. *J. Am. Chem. Soc.* **1967**, *89*, 1036. Doany, F. E.; Hochstrasser, R. M.; Greene, B. I.; Millard, R. R. *Chem. Phys. Lett.* **1985**, *118*, 1. (b) Troe, J.; Weitzel, K.-M. *J. Chem. Phys.* **1988**, *88*, 7030.

TABLE I: Molecular Structures, Emission Properties as Free Molecules and in Clusters, Wavelength Origins, Emission Lifetimes, Activation Energies, and Quantum Yields for DHP Formation for the Molecules Investigated in This Work

molecule	emission		origin, nm	fluorescence lifetime, ns	DHP E_a , kcal/mol	$\Phi_{cis\text{-}DHP}$
	isolated	cluster				
<i>cis</i> -stilbene	no	yes	>343.5	17.2	1.2 ¹⁶	10% (30%) ^{4,16}
<i>trans</i> -stilbene	yes	yes	310.14 ¹⁰	2.7 ¹⁰		
DPC-4	yes	yes	322.6	7.3	<5.9	~0%
DPC-5	no	yes	>335.0	14.7	2.6 ¹⁶	50% ¹⁶
DPC-6	no	no	?	?	?	high
DBS	yes	yes	304.4	?	?	0%



ing-Oxtoby theory for activationless electronic relaxation in solution,²⁷ they nevertheless suggested that the observed nonradiative decay directly measures motion along the reaction coordinate, which has no significant barrier when the solvent is propanol.³

In a preliminary report of the present work, new dimensions in *cis*-stilbene structure and dynamics were explored by measuring the spectra and dynamics of several *cis*-stilbene homologues such as 1,2-diphenylcycloalkenes and dibenzosuberene, which contain the same chromophore as *cis*-stilbene but are structurally prevented from undergoing *cis*-*trans* isomerization.⁴ The nonradiative decays of 1,2-diphenylcyclopentene (DPC-5) and 1,2-diphenylcyclohexene (DPC-6) indicate that the conrotatory photocyclization to the corresponding dihydrophenanthrene (DHP) structure is fast and that it can effectively compete with *cis*-*trans* isomerization.^{4,25} DPC-4 is fluorescent because the barrier to photocyclization is high, effectively preventing the formation of the corresponding DHP structure. Nevertheless, the vibrationally resolved spectrum of this molecule displays long progressions in the phenyl bending and twisting modes, indicating that the initial motion on the excited surface is along the reaction coordinate for production of DHP.⁴

In the present work, the experimental DPC-4 fluorescence excitation spectrum is modeled in an effort to derive an empirical excited-state potential surface for the symmetric (in-phase) bend, α , and the symmetric (in-phase) phenyl twist, ϕ , vibrations (see Figure 1). For the remainder of the paper, these low-frequency vibrations will be referred to as the "bend" and the "phenyl twist" motions; however, it should be kept in mind that both of these vibrational modes involve the concerted motion of *both* of the phenyl rings. The "symmetric" label implies that the overall C_2 symmetry of the molecule is preserved by these vibrations. Finally, although the normal modes can be characterized as having mostly bend or mostly phenyl twist character, the bend and the phenyl twist are not themselves pure motions in the molecule but are weakly mixed with one another in the true normal modes.

The structural similarity of the diphenylcycloalkenes and *cis*-stilbene can be exploited to derive excited-state surfaces for DPC-5, DPC-6, and *cis*-stilbene from the surface found for DPC-4. The key to extrapolating the DPC-4 surface to other molecules lies in parametrizing the potential surface in terms of the generalized forces that contribute to the structure and properties of all the molecules. These forces include, for example, the H_2 - H_2 repulsive interaction, the conjugative force favoring planarity in the π -system, and the C_2 - C_2 attractive interaction on the excited state. Several workers have constructed similar empirical force fields for a variety of different molecules in the past;²⁸⁻³² however, the present study enjoys the advantage of having detailed information

about the vibrations on the S_1 state of DPC-4 with which to assign the parameters. In addition, earlier studies were mostly concerned with modeling the ground electronic state, whereas here the objective is an accurate excited-state surface. With a quantitatively accurate DPC-4 surface, it is then much more likely that the extrapolated surfaces for the other molecules will at least be qualitatively representative of their true excited-state surfaces in these coordinates.

The remainder of the paper is organized as follows. A description of the experimental apparatus and a presentation of experimental results and analysis are given in section II. These results form the foundation of the theoretical analysis, which begins in section III with a description of the methods used to (i) find the G matrix elements for the bend and phenyl twist vibrations, (ii) construct the empirical potential surface for DPC-4, and (iii) simulate the observed spectrum from the empirical surface. Section IV follows with a discussion of the theoretical fitting results, with an emphasis on the implications for the excited-state dynamics of the 1,2-diphenylcycloalkenes and *cis*-stilbene. Finally, the results of this work are summarized in section V.

II. Experimental Studies

A. Experimental Procedure. The experimental apparatus has been described previously in detail.^{4,23,24,33} Briefly, an excimer-pumped dye laser is used to excite the *cis*-stilbene and related molecules in a free jet expansion. The laser-induced fluorescence spectra are obtained by collecting the total fluorescence and detecting with a photomultiplier tube (PMT). The emission spectra are recorded by dispersing the fluorescence in a 250-mm monochromator and detecting with an optical multichannel analyzer. The lifetimes are measured by using an amplified picosecond laser system excitation laser and either a LeCroy 9400 digital oscilloscope or a Tectronix 7912 transient digitizer to record the fluorescence decays. The system time resolution is limited by the 2.2-ns response time of the Hamamatsu R758 PMT. For spectroscopy of free molecules, the sample is seeded in 1-2 atm of He, while for the spectroscopy of Ar clusters, the sample is seeded in ~2 atm of Ar. Because all of the samples are solids at room temperature, they are heated inside the molecular beam nozzle to 40-70 °C. Since most of the samples are sensitive to temperature, light, and oxygen, they are refrigerated under N_2 atmosphere and shielded from light. DPC-6, DPC-5, and DPC-4- d_0 are synthesized by using the procedure described in ref 25. DPC-4- d_{10} , which has its phenyl ring hydrogens substituted by deuterium, is synthesized from dibenzoylthane- d_{10} by reduction followed by cyclization with $LiAlH_4$ and $TiCl_3$. The precursor dibenzoylthane- d_{10} is prepared by Friedel-Crafts reaction of benzene- d_6 and fumaryl chloride, with subsequent reduction with $SnCl_2$ and $HCl(aq)$.³⁴

B. Experimental Results and Analysis. The experimental results have been presented in ref 4 and are summarized here in

(27) Bagchi, B.; Fleming, G. R.; Oxtoby, D. W. *J. Chem. Phys.* **1983**, *78*, 7375.

(28) Fischer-Hjalmars, I. *Tetrahedron* **1963**, *19*, 1805.

(29) Williams, D. E. *J. Chem. Phys.* **1966**, *45*, 3770.

(30) Imamura, A.; Hoffmann, R. *J. Am. Chem. Soc.* **1968**, *90*, 5379.

(31) Park, N. S.; Waldeck, D. H. *Chem. Phys. Lett.* **1990**, *168*, 379.

(32) Allinger, N. L.; Yuh, Y. H.; Lii, J.-H. *J. Am. Chem. Soc.* **1989**, *111*, 8551. Lii, J.-H.; Allinger, N. L. *J. Am. Chem. Soc.* **1989**, *111*, 8566, 8576.

(33) Petek, H.; Yoshihara, K.; Christensen, R. C. *J. Chem. Phys.*, submitted.

(34) Baily, P. S.; Lutz, R. E. *J. Am. Chem. Soc.* **1948**, *70*, 2412. Baumstark, A. L.; Bechara, J. H.; Semigran, M. J. *Tetrahedron Lett.* **1976**, 3265.

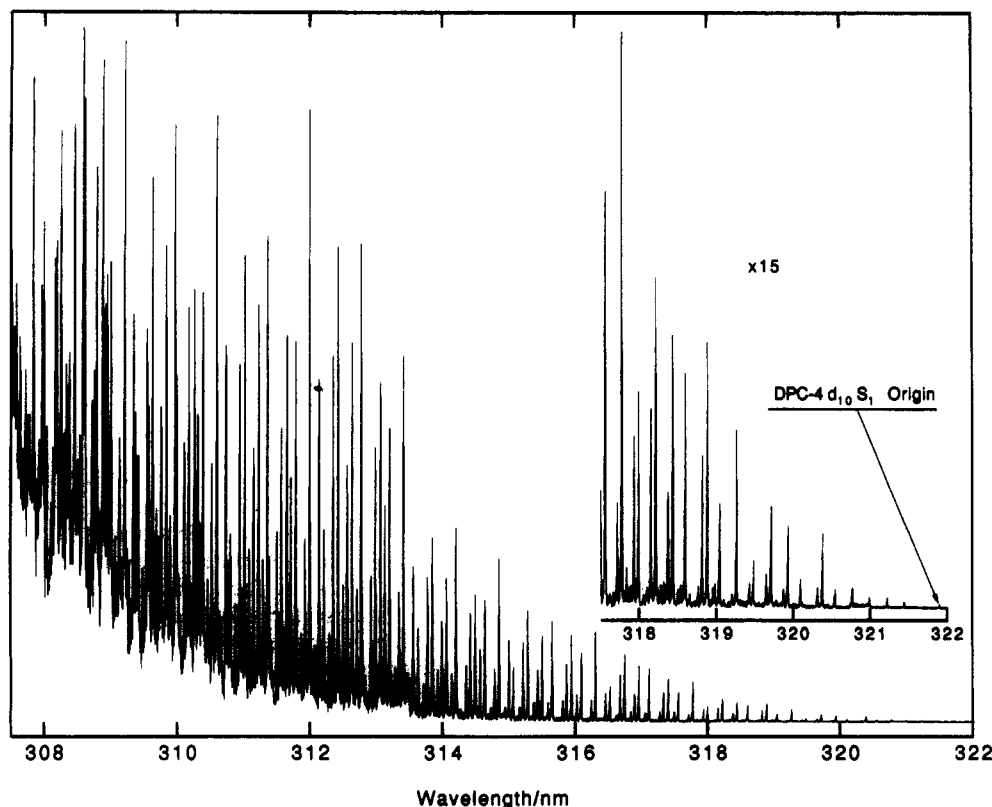


Figure 2. Experimentally observed laser-induced fluorescence spectrum of DPC-4- d_{10} . The spectra is measured in 3-nm overlapping segments that are normalized in intensity and combined in the present spectrum. Almost all of the lines can be assigned to only fundamentals, overtones, and combination bands of the phenyl in-plane, ω_i , and out-of-plane bends, ω_o , and the symmetric phenyl twist, ω_s (the ω_o assignment is tentative). The observed long progressions and the low intensity of the origin show that there is a large change in geometry between S_0 and S_1 states. A more complete discussion of these assignments is presented in ref 4.

TABLE II: Comparison between Observed and Calculated Vibrational Frequencies (cm^{-1}) on the S_1 State of DPC-4- d_0 and - d_{10}

DPC-4- d_0		DPC-4- d_{10}		assignment
obsd	calcd ^a	obsd	calcd ^a	
46.7		43.9	44.3 ^b	ω_o , out-of-plane bend
70.6	71.5	65.5	65.5	ω_s , sym phenyl twist
151.4	152.0	146.9	144.5	ω_i , in-plane bend

^aCalculated frequency from empirical potential surface reported in sections III and IV. ^bCalculated isotope shift based on observed DPC-4- d_0 frequency.

Table I. It is found that the fluorescence properties of 1,2-diphenylcycloalkenes strongly depend on the ring size. DPC-4, for which the phenyl ring interactions are the smallest, is strongly fluorescent under isolated conditions and in Ar clusters. The low-resolution fluorescence excitation spectrum in Figure 2 shows resolved vibrational structure that rapidly increases in intensity starting at the origin of 322.6 nm (321.9 nm for DPC-4- d_{10}). As discussed in the preliminary report of this work, almost all of the lines can be assigned to fundamentals, overtones, and combination bands of in-plane phenyl bend, ω_i , out-of-plane phenyl bend, ω_o , and symmetric phenyl twist, ω_s .⁴ The frequencies of the fundamental bands are given in Table II. The envelope of the spectrum is determined by the in-plane phenyl bend, which increases in intensity for higher overtones up to $\nu = 10$, at the high-energy limit of the spectrum in Figure 2. Spectra taken below the reported region continue to increase in intensity beyond 299 nm. There are no obvious lines that can be assigned to high-frequency modes such as C=C stretching probably because the fundamentals of these modes have much smaller Franck-Condon factors than the nearby overtones and combination bands of the low-frequency modes. The assignments of the low-frequency modes for DPC-4- d_0 and - d_{10} are shown in Figure 3. Although there is a close resemblance between the spectra, the intensity distributions are somewhat different, especially for ω_s , the symmetric phenyl twist, which has a considerably longer progression in DPC-4- d_0 than

in - d_{10} . This may be explained by the slight difference in the 2:3 Fermi resonance and therefore intensity sharing between ω_s and ω_o . Further discussion of the assignment and spectral simulation of the low-frequency modes ω_s and ω_i will be given in the theoretical sections (III and IV) of the paper.

The emission spectra from DPC-4 under isolated conditions and in clusters are shown in Figure 4. When the emission is measured from low overtones of the ω_i ($\nu = 2$ or 3), the in-plane bend, poorly resolved C=C stretching structure can be observed; but when the emission is from higher overtones or from combination bands with ω_o and ω_s , the emission is structureless. The emission spectrum from DPC-4 in large Ar clusters is red shifted with respect to the free molecule spectrum because of the cluster solvent shift and because rapid vibrational relaxation dissipates excess vibrational excitation into cluster van der Waals modes, which effectively cools the molecule to the cluster temperature on a time scale that is much faster than emission.²³

The DPC-4 lifetimes are measured at several excess energies. The results reported in Table I are for molecules in Ar clusters and free molecules at low excess energies ($<1000 \text{ cm}^{-1}$). Above 2500 cm^{-1} of excess energy, the lifetime is faster than the experimental resolution. The lifetime may decrease because a nonradiative channel such as photocyclization may be accessible at higher excess energies. The estimate of the barrier for photocyclization of DPC-4 in Table I is based on this observation. Since the observed lifetimes are at the limit of the present apparatus, the excess energy dependence of the lifetime is not studied in detail.

DPC-5 and -6 are also investigated under isolated conditions and in Ar clusters. Under isolated conditions both are nonfluorescent; however, when DPC-5 is solvated in Ar clusters, a strong emission with ~ 14.7 -ns lifetime is observed. These observations are consistent with previous measurements by Penn and co-workers for the same molecules in room temperature and cryogenic solutions.²⁵ In that work, DPC-4 was found to be fluorescent even in room-temperature solution, DPC-5 and *cis*-stilbene are fluorescent only at 77 K, and DPC-6 is nonfluorescent

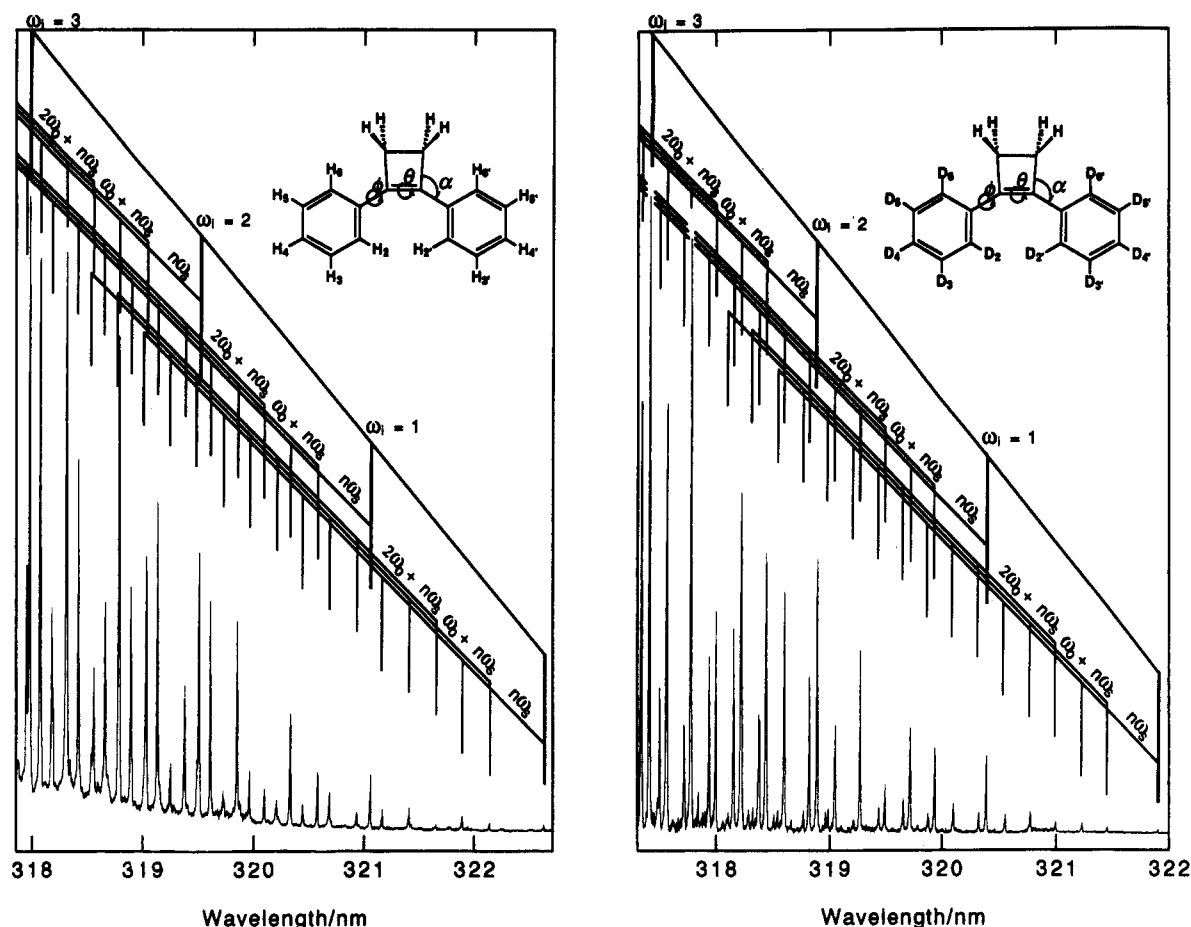


Figure 3. Low-energy region of DPC-4- d_0 and - d_{10} laser-induced fluorescence spectra. The vertical and horizontal scales have been adjusted so that the intensity of the strongest band is the same in both spectra, and the spacing between the peaks in the ω_i progression is the same for both isotomers. The indicated assignments show how most of the lines can be assigned to progressions in overtones and combination bands of ω_i , ω_0 , and ω_1 . Most of the weaker lines that occur as weak satellites on the main progressions can be assigned to states that originate from $3\omega_0$ or $4\omega_0$. The difference in the slope of DPC-4- d_0 and - d_{10} spectra is either an experimental artifact (possibly a difference in the beam temperature) or a major difference in intramolecular vibrational coupling that results from minor differences in vibrational frequencies of the two isotomers.

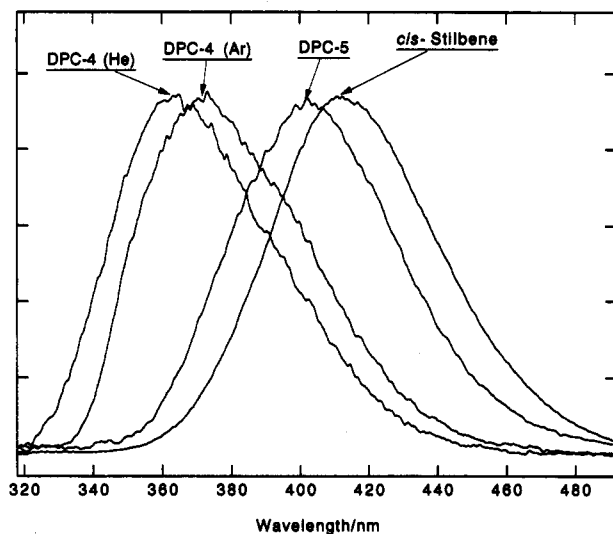


Figure 4. Comparison of emission spectra from DPC-4, DPC-5, and *cis*-stilbene. The DPC-4 (Ar), DPC-5, and *cis*-stilbene are measured in Ar expansions (1600 Torr of Ar stagnation pressure) under conditions that favor solvation of the chromophore in large clusters. The DPC-4 (He) spectrum is measured in a He expansion (1600 Torr stagnation pressure) from isolated molecules with $\sim 600\text{-cm}^{-1}$ excess vibrational energy. The progressive red-shift of the emission maximum for the three molecules is a qualitative measure in the extent of conformational change in the excited state.

under any circumstances.²⁵ The emission spectra from *cis*-stilbene and DPC-5 in Ar clusters shown in Figure 4 closely resemble cryogenic solution spectra of Penn and co-workers.²⁵

III. Theoretical Modeling of Low-Frequency Motions

The theoretical treatment of the low-frequency motions that participate in the rich excited-state dynamics of *cis*-stilbene and the 1,2-diphenylcycloalkenes is greatly complicated by the size of the molecules. Because they contain more than 70 vibrational degrees of freedom, it is impossible to model their dynamics in complete detail. Fortunately, the high-resolution spectra of DPC-4 (Figure 3) and its deuterated analogue indicate that below an energy of $\sim 1000\text{ cm}^{-1}$ or so only a handful of vibrations are activated by the electronic transition. On the basis of the spectroscopic analysis of similar molecules, including *trans*-stilbene^{15,20} and benzophenone,³⁵⁻³⁷ these progressions have been attributed to the symmetric bend, ω_i (151.4 cm^{-1}), the symmetric phenyl twist, ω_s (70.6 cm^{-1}), and, tentatively, to the out-of-plane phenyl bend, ω_o (46 cm^{-1}).⁴ For the remainder of the paper, the focus will be on the in-plane bend and the phenyl twist (see Figure 1 for a drawing of these coordinates); however, the effects of motion in the ethylenic torsion coordinate, θ , which leads to *cis*-*trans* isomerization in stilbene, will also be discussed.

Although the spectra indicate that only a couple of vibrational degrees of freedom need be included, there remain several challenges to overcome. First of all, these vibrations involve the collective motion of many atoms at once, meaning that their effective masses, or G matrix elements,³⁸ must be determined. In

(35) Holtzclaw, K. W.; Pratt, D. W. *J. Chem. Phys.* **1986**, *84*, 4713.

(36) Kamei, S.; Sato, T.; Mikami, N.; Ito, M. *J. Phys. Chem.* **1986**, *90*, 5615.

(37) Frederick, J. H.; Heller, E. J.; Ozment, J. L.; Pratt, D. W. *J. Chem. Phys.* **1988**, *88*, 2169.

(38) Wilson, E. B., Jr.; Decius, J. C.; Cross, P. C. *Molecular Vibrations*; McGraw-Hill: New York, 1955. Meister, A. G.; Cleveland, F. F. *Am. J. Phys.* **1946**, *14*, 13.

general, the *G* matrix elements for these kinds of motions have not been tabulated—their determination is complicated by the fact that the phenyl twisting motions generate internal angular momentum that must be separated from rotational motion in the molecule.

Second, and perhaps more critically, no reliable potential surfaces exist for the low-frequency vibrations in these molecules. Electronic structure calculations are presently unable to treat quantitatively the low-frequency vibration of molecules this large in the ground electronic state, much less the excited states. In addition, though semiempirical surfaces based on quantum consistent force field (QCFF) calculations have been generated for stilbene,^{15,39} it has not been possible to construct quantitative empirical surfaces due to a lack of detailed information about the excited states. Although detailed spectroscopic information for the DPC-4 and *trans*-stilbene excited states is now available, there is still no direct vibrationally resolved information about the excited states of DPC-5, DPC-6, or *cis*-stilbene. Because of the *C*₂ symmetry of these molecules, their surfaces should involve multiple minima along the twist coordinate, not to mention the various minima proposed along the ethylenic torsion coordinate (Figure 1). If the barriers between these multiple wells are low, then the theoretical calculation of the molecular spectra cannot easily be done using a basis set diagonalization, and one must resort to more powerful techniques.

The approach used in the present study, then, will involve several steps. First of all, expressions for the kinetic energy of the bend and twist vibrations will be derived so that the correct mass factors can be used in the subsequent analysis. Then, with the high-resolution spectrum of DPC-4, an empirical potential surface will be constructed for the *S*₁ state that reproduces the vibrational frequencies, isotope shifts, and relative intensity patterns for the bend and phenyl twist. The eventual goal is to apply the knowledge gained from the DPC-4 spectrum to finding a representation of not only the DPC-4 *S*₁ state but also the DPC-5, DPC-6, and *cis*-stilbene *S*₁ states as well. To do this, the empirical surface should model the fundamental forces in these molecules, such as the nonbonded H–H repulsive interaction that causes the phenyl rings to twist out of the plane. Only in this way can one hope to use the empirical approach to obtain structural and dynamical information about the excited-state surfaces of molecules other than DPC-4.

Although the aim is to treat these molecules as accurately as possible, a number of approximations and assumptions are necessary. Throughout the present treatment, all bond lengths and angles in the molecules will be frozen, with the exception of α and ϕ . This approximation relies on an effective adiabatic separation between these vibrations (the bend and the twist) and the other, higher frequency, vibrations in the molecule. The phenyl rings will be frozen as regular hexagons with no distortion, and all bond lengths will be set at their *S*₀ values with the exception of the ethylenic bond C₆=C₇. Since this bond is lengthened by the excitation, it has been assigned a length of 1.43 Å, which is roughly midway between its length in the ground state (1.34 Å) and the average length of a C–C single bond (1.52 Å) and is consistent with previously reported values.^{15,39,40} The twist about the ethylenic bond, which varies between 6.7° and 10.3° in these molecules²⁵ in the ground electronic state, is held constant at the *S*₀ values for all the calculations described. The twist mode is undoubtedly activated by the electronic transition, but its excursions are limited by the restrictive geometry of the cycloalkenyl rings.

Finally, despite its presence in the DPC-4 spectrum, the 46-cm⁻¹ mode has been omitted from the analysis since its assignment remains tentative. This omission leads to the implicit neglect of coupling between the 46-cm⁻¹ vibration and the in-plane bend and phenyl twist and, therefore, could affect the shape of the resulting potential function. In particular, the force constants and an-

harmonicity of the other two vibrations, as well as the final expressions for the *G* matrix elements, would be slightly different were this mode included. If the tentative assignment of the 46-cm⁻¹ progression is correct, then the inclusion or omission of this vibration could also affect the barrier to photocyclization and the dynamics leading to this isomerization channel in stilbene; however, the large effective mass of this mode and the distribution of intensities in its progressions indicate that its displacement on the excited-state surface is small so it is unlikely to play a major role in the photoisomerization dynamics.

To model the photocyclization reaction on the excited-state surface, a bonding interaction between the C₂ and C₇ carbons (see Figure 1) has been included and is discussed in detail below.¹⁴ In the modeling of this interaction, the assumption has been made that the formation of dihydrophenanthrene (DHP) product in the excited state occurs on a single adiabatic electronic surface. There is no solid evidence one way or the other to support or refute this assumption: measurements have implicated a small barrier (~1.2 kcal/mol)¹⁶ to DHP formation for excited *cis*-stilbene, though an extended Hückel calculation indicates there is no barrier.¹⁴ Because C–C bond formation between the phenyl rings involves a change in the hybridization of the C₂ and C₇ carbons and breaks the aromaticity of the phenyl rings, the range of this interaction has been reduced from the usual C–C bonding interaction.

In the remainder of this section, we describe the theory used to derive the proper classical kinetic energy expressions for the symmetric bend and twist and discuss in detail the various empirical potential terms used to model the *S*₁ state of DPC-4.

A. Kinetic Energy Expressions. When DPC-4 is elevated to the excited-state potential surface, it is displaced from equilibrium along several coordinates including the symmetric phenyl twist coordinate, ϕ . As it begins to vibrate in this coordinate, it generates vibrational angular momentum along the *C*₂ symmetry axis of the molecule. If the molecule initially has no total angular momentum, it must rotate in an opposite sense to compensate for the angular momentum generated by the twist vibration. The effective mass of the twist vibration is generally reduced by this compensating rotation. In the more commonly encountered instance of bond-stretching vibrations, this effect does not occur and the effective mass can be simply treated as the reduced mass of the two atoms forming the bond. To find the correct mass corresponding to a given vibration, an expression for the kinetic energy in the absence of total angular momentum, i.e., $\mathbf{L} = 0$, must be found.⁴¹

Classically, one can write the total kinetic energy of a vibrating and rotating molecule as⁴²

$$T = \frac{1}{2}\omega \cdot \mathbf{I} \cdot \omega + \omega \cdot \boldsymbol{\ell} + T_{\text{vib}} \quad (3.1)$$

where ω is the rotational angular velocity of the molecule's axis frame, \mathbf{I} is the moment of inertia tensor in that axis frame, $\boldsymbol{\ell}$ is the internal angular momentum of the molecule, defined as

$$\boldsymbol{\ell} = \sum_k m_k (\mathbf{r}_k \times \dot{\mathbf{r}}_k) \quad (3.2)$$

(the sum is over all atoms), and T_{vib} is the kinetic energy of the molecule relative to its axis system. In eq 3.1, the first term represents rotational energy, the last term is vibrational kinetic energy, and the middle term is a vibration–rotation coupling term. With use of the fact that rotational angular momentum is given by $\mathbf{J} = \mathbf{I} \cdot \omega$ and total angular momentum $\mathbf{L} = \mathbf{J} + \boldsymbol{\ell}$, eq. 3.1 can be rewritten as⁴³

$$T = \frac{1}{2}\mathbf{L} \cdot \mathbf{I}^{-1} \cdot \mathbf{L} - \frac{1}{2}\boldsymbol{\ell} \cdot \mathbf{I}^{-1} \cdot \boldsymbol{\ell} + T_{\text{vib}} \quad (3.3)$$

Now, the total angular momentum appears explicitly in the kinetic energy expression and can be set equal to zero. The remaining two terms depend only on internal (vibrational) coordinates and

(39) Negri, F.; Orlandi, G.; Zerbetto, F. *J. Phys. Chem.* **1989**, *93*, 5124.

(40) Fischer, G.; Seger, G.; Muskat, K.; Fischer, E. *J. Chem. Soc., Perkin Trans. 2* **1975**, 1569.

(41) Cross, P. C.; Van Vleck, J. H. *J. Chem. Phys.* **1933**, *1*, 350.

(42) Allen, H. C., Jr.; Cross, P. C. *Molecular Vib-Rotors*; Wiley: New York, 1963.

(43) Frederick, J. H.; McClelland, G. M.; Brumer, P. *J. Chem. Phys.* **1985**, *83*, 190.

TABLE III: Equilibrium Configurations Used in Computing Effective Masses and in Constructing Empirical Potential Surfaces for DPC-4, DPC-5, DPC-6, and *cis*-Stilbene^a

	DPC-4		DPC-5		DPC-6		<i>cis</i> -SB	
	S ₀	S ₁	S ₀	S ₁	S ₀	S ₁	S ₀	S ₁
α	136.5	133.4	128.6	124.5	125.0	118.7 ^b	129.5	123.9
ϕ	~21 ^c	25.7	~46 ^c	27.7	~47 ^c	25.5	43.2	26.8
θ^d		10.3		7.5		6.7		9.0
γ^d		93.0		110.8		123.2		118.0 ^e
α_{eq}		133.5		124.6		119.0		124.0

^aSee Figures 1 and 5 for a description of the angles—all angles are given in degrees. ^bThese angles do not correspond to a minimum on the potential surface; they represent the minimum in DPC-6 in the absence of the C₂–C₂ bonding interaction. ^cThis is the average value from the observed range.²⁵ ^dValues used are the same for both electronic states. ^eThis is the C_c–C_c–H_c bond angle. ^f α_{eq} is defined by eq 3.12. These parameters used only in the construction of empirical potentials for the S₁ state.

represent a kinetic energy expression for the vibrations in the absence of rotation:

$$T = T_{\text{vib}} - \frac{1}{2}\dot{\ell} \cdot \mathbf{I}^{-1} \cdot \dot{\ell} \quad (3.4)$$

Since the choice of an internal axis frame directly affects the magnitude of ℓ (for instance, the Eckart frame^{42–44} tends to reduce its magnitude), this will have a bearing on the relative magnitude of these two terms; however, their sum, T , will be same regardless of the choice of molecule-fixed coordinates.

The appropriate kinetic expressions for the symmetric bend and twist vibrations can now be derived by using a straightforward prescription based on eq 3.4. The details of this procedure will be spelled out in a forthcoming publication,⁴⁵ so only a brief outline is sketched out here. First, the molecule is placed in an arbitrary Cartesian body-fixed frame whose origin corresponds to the center of mass of the molecule. Within this axis system, the positions of all the atoms are expressed in terms of fixed bond lengths and angles, q_0 , and in terms of the internal coordinates to be treated, q (in this case, $q = \alpha, \phi$). From these expressions, the Cartesian velocities of all the atoms are expressed in terms of q_0, q , and \dot{q} , and the internal kinetic energy is found by computing $T_{\text{vib}} = \frac{1}{2} \sum_k m_k \dot{\mathbf{r}}_k \cdot \dot{\mathbf{r}}_k$, where the summation is over all the atoms and $\dot{\mathbf{r}}_k$ is the Cartesian velocity of the k th atom. Next, the moment of inertia tensor, \mathbf{I} , is written in terms of the internal coordinates q_0 and q , and the internal angular momentum is computed as a function of internal coordinates and velocities by using eq 3.2. Finally, with use of eq 3.4, the expression for the vibrational kinetic energy is found and placed in the form

$$T = \frac{1}{2} \dot{\mathbf{q}} \cdot \mathbf{M}(\mathbf{q}; q_0) \cdot \dot{\mathbf{q}} \quad (3.5)$$

in which the matrix, \mathbf{M} contains the expressions for the masses of the different internal coordinates and generally will be a function of the internal coordinates (as indicated) and not a constant.

To obtain the \mathbf{G} matrix elements, one must express the kinetic energy in Hamiltonian form, rather than the Lagrangian form given in eq 3.5.⁴⁶ This involves simply inverting the matrix \mathbf{M} , so $\mathbf{G} = \mathbf{M}^{-1}$, and

$$T = \frac{1}{2} \dot{\mathbf{p}} \cdot \mathbf{G}(\mathbf{q}; q_0) \cdot \dot{\mathbf{p}} \quad (3.6)$$

where the elements of \mathbf{p} are the internal momenta conjugate to the coordinates q .⁴⁶ In practice, the expressions for the matrix elements of \mathbf{M} are quite complicated (see below), and the matrix inversion to find \mathbf{G} is correspondingly difficult. Rather than perform this step algebraically, the coordinate-dependent masses are computed at the equilibrium configuration, and these “average values” for the masses are used to determine constant \mathbf{G} matrix elements for subsequent calculations. This approximation is reasonably good for the twist mode where the masses vary by ~1% or less over the full range of phenyl twist angles. The mass of the bend is more sensitive to the geometry of the molecule; nevertheless, it varies by ≤10% over the range of angles (110° < α < 140°) explored by the dynamics of these molecules on the excited state.

The corresponding derivation of the quantum kinetic energy operator is considerably more difficult due to the coordinate dependence of the \mathbf{G} matrix elements and the noncommutivity of \mathbf{q} and \mathbf{p} .⁴⁷ For this reason, the “averaged” constant masses along with the substitution $\mathbf{p} \rightarrow -i\hbar\partial/\partial\mathbf{q}$ are used when converting the classical kinetic energy expression to a quantum kinetic energy operator. The quantum corrections^{48,49} to the classical Hamiltonian for molecular systems are typically proportional to $1/\mu$ —for the present vibrations, the effective mass μ is large and the correction terms are expected to be small.

For the symmetric bend and symmetric twist modes, the following expression is found for the Lagrangian form of the kinetic energy:⁴⁵

$$T = \frac{1}{2} \left\{ (\mu_0 + 2\mu_\phi + \mu_\beta) + \mu_\phi \cos^2 \phi - \left[\frac{(\mu_0 + \mu_\phi)^2}{Mr_t^2} \cos^2 \alpha + \frac{1}{I_{zz}} (\mu_\phi \cos \alpha \sin \phi \cos \phi)^2 \right] \cos^2 \frac{\theta}{2} \right\} \dot{\alpha}^2 + \frac{1}{2} \mu_\phi \left(1 - \frac{\mu_\phi}{I_{zz}} \sin^2 \alpha \times \cos^2 \frac{\theta}{2} \right) \dot{\phi}^2 - \left(\frac{\mu_\phi}{I_{zz}} \sin \alpha \cos \alpha \sin \phi \cos \phi \cos^2 \frac{\theta}{2} \right) \dot{\alpha} \dot{\phi} \quad (3.7)$$

Here, the various constant factors that appear are given by the expressions

$$\begin{aligned} \mu_0 &= (12m_C + 10m_H)r_t^2 \\ \mu_\phi &= 12m_C r_o r_o + 2m_H r_t (r_H + 6r_o) \\ \mu_\beta &= 18m_C r_o + 2m_H [r_H^2 + (r_H + 3r_o)^2] \\ \mu_\phi &= 6[m_C r_o^2 + m_H (r_o + r_H)^2] \quad M = 16m_C + 14m_H \end{aligned} \quad (3.8)$$

and the I_{zz} element of the moment of inertia tensor has the form

$$I_{zz} = I_{zz}^{(cb)} + (\mu_0 + 2\mu_\phi + \mu_\beta + \mu_\phi \sin^2 \phi) \cos^2 \alpha + \mu_\phi \sin^2 \alpha + \left(\frac{r_C^2}{4r_t^2} \right) \mu_0 - 2 \left(\frac{r_C}{2r_t} \right) (\mu_0 + \mu_\phi) \cos \alpha \quad (3.9)$$

Because these vibrations preserve the C₂ symmetry of the molecule, only the ℓ_z component of the internal angular momentum is nonzero (the z axis is chosen to be along the symmetry axis) and the I_{xz} and I_{yz} elements of \mathbf{I} are zero. Thus, the second term in eq. 3.4 reduces to $-\ell_z/2I_{zz}$. In eq 3.9, $I_{zz}^{(cb)}$ represents the moment of inertia of the cycloalkene ring about the z axis. The values used for the various bond lengths and masses are identified in Figure 5. In addition, the excited-state configurations used in computing the effective masses for the bend and twist are listed in Table III along with previously reported values for the equilibrium geometry of the ground electronic state.²⁵

B. Empirical Potential Energy Surfaces for S₁. There are two major goals in the present effort to construct an empirical surface for the S₁ state of DPC-4: (i) to reproduce the high-resolution spectral data including both vibrational frequencies and relative

(44) Eckart, C. *Phys. Rev.* **1935**, *47*, 552.

(45) Hadder, J. E.; Frederick, J. H., manuscript in preparation.

(46) Goldstein, H. *Classical Mechanics*, 2nd ed.; Addison-Wesley: Reading, MA, 1980.

(47) Podolsky, B. *Phys. Rev.* **1928**, *32*, 812.

(48) Watson, J. K. G. *Mol. Phys.* **1968**, *15*, 479.

(49) Frederick, J. H.; McClelland, G. M. *J. Chem. Phys.* **1986**, *84*, 876.

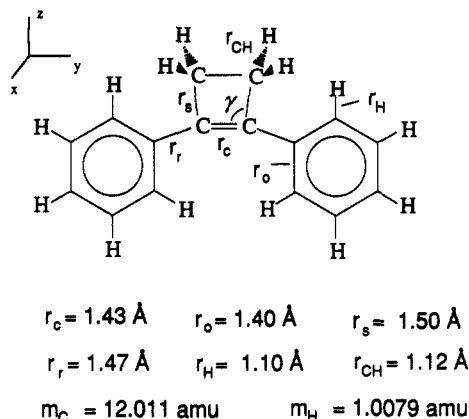


Figure 5. Identification of bond length parameters used in the kinetic energy expressions for DPC-4. All indicated bond lengths are held fixed in the present work, and the molecular C_2 symmetry is maintained in the simulations. The phenyl rings are treated as regular hexagons, and the cyclobutene ring is held in a rigid configuration for all the calculations reported. The angle γ is used to assign the parameter α_{eq} in the bend potential according to eq 3.12.

intensities; (ii) to parametrize the surface in terms of general forces that are nonspecific to DPC-4 but will allow a generalization to other similar molecules.

The ground-state phenyl ring geometry of all of these molecules (DPC-4, -5, and -6 and *cis*-stilbene) is determined by a delicate balance of two forces: the π -system conjugation, which favors planar geometries, and the nonbonded H-H steric repulsion, which favors nonplanar geometries. Each molecule finds a suitable compromise geometry that is dictated in large part by the geometry of the central cycloalkenyl ring (see Table III). In DPC-4, where the cyclobutene ring artificially causes the central bond angles to be quite large ($\alpha_0 = 136.5^\circ$), the two phenyl rings are able to attain a configuration much closer to planar than in DPC-6 where the central bond angles are much smaller ($\alpha_0 = 125^\circ$). The excited singlet-state geometry will be dictated by a similar balance of conjugative and steric forces, with the additional effect of a bonding interaction between C_2 and C_2' which leads to the photocyclization product DHP (and its cycloalkyl analogues).⁴ In the ground state, the C_2 - C_2' interaction is a repulsive one as explained above.

To maintain flexibility, the empirical surface will model each of these important interactions separately, allowing the geometry of each of the diphenylcycloalkenes to dictate how these forces balance one another. Thus, the potential has the form

$$V = V_{\text{bend}} + V_{\text{conj}} + V_{\text{HH}} + V_{\text{CC}} \quad (3.10)$$

where V_{bend} is the potential for the bond angle α , V_{conj} represents the conjugative forces, V_{HH} models the steric repulsion between various pairs of nonbonded H atoms, and V_{CC} describes the bonding interaction between C_2 and C_2' .

The DPC-4 spectrum contains a long progression of almost equally spaced lines in the bend mode, indicating that the mode is fairly harmonic and that its equilibrium position in S_1 is greatly displaced from that in S_0 . In the present work, V_{bend} is modeled as a harmonic oscillator:

$$V_{\text{bend}}(\alpha) = \frac{1}{2}k_\alpha(\alpha - \alpha_{eq})^2 \quad (3.11)$$

in which the "equilibrium" angle, α_{eq} , is assigned separately for each molecule to be

$$\alpha_{eq} = \frac{1}{2}(2\pi - \gamma) \quad (3.12)$$

where γ is the internal angle of the cycloalkenyl ring at the ethylene carbon, C_e (see Figure 5). Table III lists the value of γ for each of the molecules studied—these values were derived from molecular mechanics (MM2) calculations⁵⁰ for the isolated molecules.

Note that the parameter α_{eq} does not automatically determine the equilibrium value of the bend angle since there are forces exerted on α by all of the other interactions in the empirical potential. Nevertheless, the final equilibrium bond angle is often close (within 0.5°) to the value of α_{eq} . Once the assignment of α_{eq} has been made via eq 3.12, only k_α remains as an adjustable parameter for this part of the potential. In reality, the bend potential probably includes anharmonic terms as well, and the resulting fit of the spectral data could certainly be improved by their inclusion. However, there are many approximations involved in the present approach and the addition of anharmonic terms to V_{bend} would not qualitatively change the present results.

Conjugative forces have been the subject of several early theoretical investigations of large molecules with extended π -systems, especially biphenyl.²⁸⁻³⁰ One of the results of these studies is that the preference for a planar geometry is well-described by a truncated Fourier series in the twist angle, ϕ .^{28,29} As a result, V_{conj} is represented by the two-parameter function

$$V_{\text{conj}}(\phi) = \frac{1}{2}V_2(1 - \cos 2\phi) + \frac{1}{2}V_4(1 - \cos 4\phi) \\ = V_2 \sin^2 \phi + V_4 \sin^2 2\phi \quad (3.13)$$

In eq 3.13, both V_2 and V_4 are adjustable parameters to be found by fitting the experimental spectrum. For this choice of function, V_2 determines the height of the barrier to phenyl ring rotation about the C_e - C_1 bond in the absence of steric interactions. V_4 determines how "flat" or sharp the barriers to phenyl twisting motion are—the barriers become flatter and the wells steeper as V_4 increases. If one were also modeling the ground-state potential, these terms would probably reflect the greatest change between the two electronic states because the transition primarily affects the conjugated π -system.

Nonbonded H atom repulsive forces are common to a plethora of different molecules; however, there seems to be little consensus as to an appropriate empirical form to represent these forces.^{28,32,51} Rather than concoct yet another H-H nonbonded potential, the potential given in the molecular mechanics (MM3) force field³² for this interaction is used. The MM3 force field correctly predicts the geometries of a large number of molecular systems in their ground electronic state, and this interaction is not expected to be significantly different in the excited singlet state. One latent problem with the MM3 function for V_{HH} is that, at small H-H separations ($<1.1 \text{ \AA}$ or so), the potential turns over and becomes strongly attractive. To prevent this from becoming a factor in the present study potential, an exponential is fit to the MM3 function at the inflection point so that the potential and its first derivative are continuous. As a result

$$V_{\text{HH}} = \sum_i V_{\text{vdw}}[r_i(\alpha, \phi)] \quad (3.14a)$$

where

$$V_{\text{vdw}}[r_i(\alpha, \phi)] = \begin{cases} V_r e^{-\beta r_i} + (C/r_i^6) & r_i > 1.1506 \text{ \AA} \\ V' e^{-\beta' r_i} & r_i \leq 1.1506 \text{ \AA} \end{cases} \quad (3.14b)$$

for the H-H repulsive interaction.

In eq 3.14a, the sum is over all the pairs of nonbonded H-H atoms to be treated and the H-H distances, r_i , are all functions of both α and ϕ . In the present study, 12 such pairs, including the four interactions between the phenyl rings involving the H atoms at the 2 and 6 positions, and 8 interactions between the 2- and 6-position hydrogens on each phenyl ring and the four nearest hydrogens on the cycloalkenyl ring are included. V_{HH} contains no adjustable parameters for the purposes of fitting to experiment but should be applicable to all of the molecules studied here. The parameters used in V_{HH} are listed in Table IV.

The bonding interaction between C_2 and C_2' presents new challenges. Since little or nothing is known about the strength or vibrational frequency of this bond in the excited-singlet state

(50) Allinger, N. L. *J. Am. Chem. Soc.* **1977**, *99*, 8127.

(51) Williams, J. E.; Stang, P. J.; Schleyer, P. v. R. *Annu. Rev. Phys. Chem.* **1968**, *19*, 531.

TABLE IV: Parameters Used in the V_{HH} and V_{CC} Empirical Force Fields

	V_{HH}^a		V_{CC}^b
V_c^c	$1.287 \times 10^6 \text{ cm}^{-1}$	D_{CC}	$29\,030 \text{ cm}^{-1}$
β_c^c	3.704 \AA^{-1}	β_C	5.67 \AA^{-1}
C^c	$-1.821 \times 10^4 \text{ cm}^{-1} \text{ \AA}^6$	R_{eq}	1.53 \AA
V'^d	$1.943 \times 10^5 \text{ cm}^{-1}$		
β'^d	2.553 \AA^{-1}		

^a Defined in eq 3.14. ^b Defined in eq 3.15. ^c Values are derived from the MM3 force field.³² ^d Parameters used in the short-range correction to the MM3 nonbonded H-H potential.

of DHP, general parameters for C-C single bonds have been used to model this interaction. In addition, since the bond originates as an interaction between two p-orbitals, the function has artificially been given directionality to favor configurations in which the phenyl rings allow the two p-orbitals to line up parallel to one another. This results in the function

$$V_{CC} = D_{CC}[\exp[-2\beta_c(R_{CC} - R_{eq})] - 2 \exp[-\beta_c(R_{CC} - R_{eq})]] \cos^2 [\chi(\alpha, \phi)] \quad (3.15)$$

where the isolated bond well depth, D_{CC} , is taken to be 83 kcal/mol and the equilibrium bond length R_{eq} is set at 1.53 Å (see Table IV). The Morse width parameter, β_c , is ordinarily fit to the vibrational frequency of the bond; however, here its value has been set so that the range of the interaction is relatively short to account for the otherwise untreated factors of C atom rehybridization and the loss of aromaticity caused by C-C bond formation. Interestingly, using the indicated potential parameters and an estimate of the effective mass for this bond coordinate, one obtains a vibrational frequency on the order of 700–900 cm^{-1} , which is reasonable for bonds of this type. As in V_{HH} , the C-C distance, R_{CC} , is implicitly a function of the angles α and ϕ , but only the two nearest carbon atoms (for example, 2 and 2') are treated at a time due to the imposed short range of the interaction.

The angle χ , which appears in eq 3.15, is a measure of how well the two p-orbitals on the C_2 and $C_{2'}$ atoms line up. If one forms a vector connecting the two interacting carbons, then χ is the angle between this vector and a vector normal to the plane of one of the phenyl rings (the angle made with the normal vector to the other phenyl ring is the same by symmetry). When χ is 0, then the two p-orbitals are parallel to one another and maximum overlap can be achieved; when χ is 90°, then the orbitals are perpendicular to one another and the interaction is zero, no matter how close together the C atoms are. While the true angular variation of this interaction is probably a more complicated function, the $\cos^2 \chi$ term nevertheless qualitatively reproduces the correct directionality for the C-C attractive force.

C. Fitting Procedure. As indicated, there are only three free parameters, k_α , V_2 , and V_4 , to be adjusted in fitting the experimental spectroscopic information for DPC-4. All other parameters and coordinates, including the ethylenic twist angle θ , are held fixed for the purposes of establishing the empirical potential. To test the accuracy of a given set of parameters, the eigenvalue spectrum is computed by using a time-dependent wave-packet method of the sort popularized by Heller and co-workers.^{26,52} This method works well for a wide variety of potential surfaces and is especially useful when the surface has multiple wells or is very anharmonic as is the case here.

The method is based on the fact that any given nonstationary state $|\Phi(0)\rangle$ can be expressed as a superposition of the eigenstates of the Hamiltonian⁵³

$$|\Phi(0)\rangle = \sum_n c_n |\psi_n\rangle \quad (3.16)$$

with its time dependence given by

$$|\Phi(t)\rangle = \sum_n c_n e^{-iE_n t/\hbar} |\psi_n\rangle \quad (3.17)$$

If one computes the autocorrelation function of this nonstationary state at several times during the time evolution

$$\langle \Phi(0) | \Phi(t) \rangle = \sum_n |c_n|^2 e^{-iE_n t/\hbar} \quad (3.18)$$

then this function of time can be Fourier transformed to obtain the eigenvalue spectrum

$$\int_{-\infty}^{\infty} dt e^{i\omega t} \langle \Phi(0) | \Phi(t) \rangle = \sum_n |c_n|^2 \delta(\omega - 1/\hbar E_n) \quad (3.19)$$

While the integration limits have been formally written as $\pm\infty$, in practice the integration is performed over a finite time giving something less than "δ-function" resolution to the peaks in the eigenvalue spectrum. As Heller, Imre, and co-workers have shown,^{37,54,55} a similar procedure can be adapted for the time-dependent computation of molecular spectra in which the spectrum is proportional to the left-hand side of eq 3.19 with the integration limits adjusted to correspond to shorter (than infinite) observation times. This is the procedure used to simulate the DPC-4 spectrum in the current study.

The numerical implementation of this approach depends on one's ability to generate the time evolution of a given nonstationary state. Several algorithms for doing this have been developed^{56,57}—in the present work, the method of Feit and Fleck⁵⁷ is used. Since this method is described in detail elsewhere, further description of it will not be given here. For the purposes of finding the proper potential parameters, an initial wave packet is typically propagated for 3–4 ps, which represents roughly 20 periods of oscillation in the bend vibration and ~ 10 periods in the phenyl twist vibration. This is sufficient to resolve the eigenvalues to within 2 cm^{-1} and allow a determination of the usefulness of a given set of parameters. Once a suitable set of parameters is found, a longer run of 8–9 ps is made to evaluate the energy levels to the nearest 0.5 cm^{-1} .

The relative intensities observed in the spectrum depend primarily on two factors: the displacement in the equilibrium geometry and the ratio of the vibrational frequencies for the two electronic states. Since the vibrational frequencies of the low-frequency modes of DPC-4 in the ground electronic state are not well-known, it is assumed in this study that the bend has the same frequency on both states and that the ratio of the twist frequencies is $\omega_{\text{twist}}(S_0)/\omega_{\text{twist}}(S_1) \approx 0.9$. This assignment mostly affects the "spread" of the spectral envelope and is not a critical factor in arriving at a useful fit.

The displacement between the two surfaces can be estimated for each of the two degrees of freedom by measuring the ratio of the intensities of the first two peaks in their progressions. Using the harmonic approximation for both surfaces and assuming that the normal modes are the same on both surfaces (i.e., no Duschinsky rotation), the displacement is given by

$$\Delta Q \approx \pm \left[\frac{\hbar}{\mu} \frac{(\omega_0 + \omega_1)^2}{\omega_0^2 \omega_1} \right]^{1/2} \left(\frac{I_{0 \rightarrow 1}}{I_{0 \rightarrow 0}} \right)^{1/2} \quad (3.20)$$

where ω_0 and ω_1 are the frequencies on the ground- and excited-state surfaces, respectively, μ is the effective mass of the normal mode, and the subscripts on the intensities indicate the vibrational transition measured (0 on the ground state and 0 or 1 on the excited state). One should note that this formula does not indicate in which direction the excited state surface is displaced relative to the ground-state surface. Applying this general formula to the symmetric bend and twist indicates that α is displaced by roughly

(54) Chasman, D.; Imre, D. G.; Tannor, D. *J. Chem. Phys.* **1988**, *89*, 6667. Zhang, J.; Heller, E. J.; Huber, D.; Imre, D. G.; Tannor, D. *J. Chem. Phys.* **1988**, *89*, 3602.

(55) Imre, D. G.; Zhang, J. *J. Chem. Phys.* **1989**, *139*, 89.

(56) Kosloff, R. *J. Phys. Chem.* **1988**, *92*, 2087.

(57) Feit, M. D.; Fleck, J. A., Jr.; Steiger, A. *J. Comput. Phys.* **1982**, *47*, 412. Feit, M. D.; Fleck, J. A. *J. Chem. Phys.* **1982**, *77*, 301; **1984**, *80*, 2578.

(52) Kulander, K. C.; Heller, E. J. *J. Chem. Phys.* **1978**, *69*, 2439. Heller, E. J. *Acc. Chem. Res.* **1981**, *14*, 368.

(53) See, for example: Cohen-Tannoudji, C.; Diu, B.; Laloë, F. *Quantum Mechanics*; Wiley-Interscience: New York, 1977.

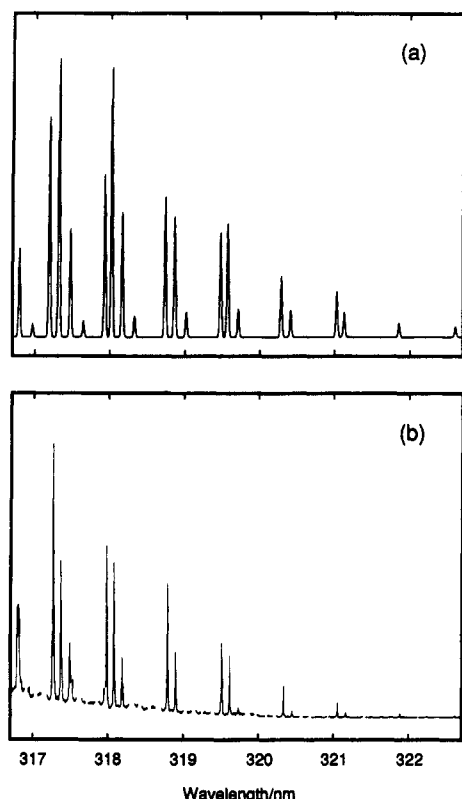


Figure 6. Comparison of the calculated (a) and observed (b) vibrationally resolved spectrum for DPC-4. To facilitate the comparison, the observed lines corresponding to states with one or more quanta in the out-of-plane bend, ω_o , have been artificially deleted, and the calculated spectrum has been energy shifted so that the two band origins coincide. The difference in line widths is purely an artifact of the calculation—calculated line widths are a function of the length of the dynamics used to compute the spectrum (see eq 3.19 and the discussion that follows).

4° , while ϕ is displaced by approximately $5\text{--}6^\circ$ in the excited state. The reproduction of these displacements by the empirical potential is restricted by the use of a limited number of adjustable parameters; however, the fitting procedure distinguishes between the different signs of the displacements (only displacements in the correct direction lead to the proper anharmonicity in the level spacing), so a unique assignment is possible.

IV. Excited-State Dynamics

A. Fitting the DPC-4 Spectrum. The calculated spectrum for DPC-4, using the potential parameters $k_\alpha = 7.52 \times 10^3 \text{ cm}^{-1}/\text{rad}^2$, $V_2 = 3210 \text{ cm}^{-1}$, $V_4 = -625 \text{ cm}^{-1}$, and $\alpha_{\text{eq}} = 133.5^\circ$ along with the nonadjusted parts of the potential, V_{HH} and V_{CC} , is shown in Figure 6a. Figure 6b shows a modified version of the experimental spectrum in which the lines associated with states having one or more quanta in the 46-cm^{-1} vibration have been artificially deleted for comparison purposes. The agreement between calculation and experiment is generally good (Table II) with the calculation yielding fundamental frequencies of 152.0 cm^{-1} for the bend and 71.5 cm^{-1} for the twist, compared to the experimental values of 151.4 and 70.6 cm^{-1} , respectively. In the isotopically substituted molecule (DPC-4- d_{10}), the calculated spectrum (not shown) gives fundamental frequencies of 144.5 and 65.5 cm^{-1} for the bend and twist, respectively, while the observed values are 146.9 and 65.6 cm^{-1} . Recall that although these modes are labeled as “bend” and “twist”, strictly speaking, the true normal modes mix these two motions a little.

A more detailed analysis reveals that the calculated spectrum is slightly more anharmonic than the experimental spectrum, with the spacing between lines decreasing by $0.5\text{--}1.0 \text{ cm}^{-1}$ for each new quantum added to the phenyl twist. In the observed spectrum, the spacing decreases by $\sim 0.1\text{--}0.2 \text{ cm}^{-1}$ with each new quantum added, resulting in a very evenly spaced set of lines. The observed harmonicity of the bend is reproduced very well by the simulated

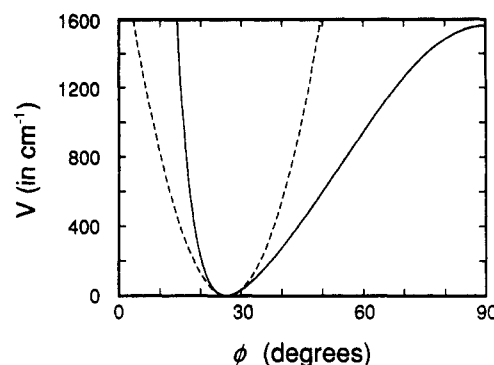


Figure 7. Cross section of the DPC-4 potential for $\alpha = \alpha_{\text{min}} = 133.4^\circ$. For comparison purposes, a harmonic potential with the same force constant at the minimum is pictured as a dashed line. Despite the fairly harmonic nature of the calculated spectrum, the twist potential for the DPC-4 S_1 state is quite anharmonic.

spectrum, as one might expect given the use of a harmonic oscillator potential in that mode. As a result, the fitted potential is probably not quite steep enough as one goes to larger phenyl twist angles but appears to represent the bend coordinate well. In addition, the constancy of the twist frequency for different numbers of bend quanta (combination bands) is well reproduced by the calculated spectrum.

It is interesting to note that although the lines in the phenyl twist progressions are evenly spaced, the potential along that coordinate is fairly anharmonic in appearance. A cross section of the DPC-4 potential with α held fixed at its equilibrium value shows that the potential is very steep on the side of small ϕ but much more gradual for larger ϕ . For comparison, this cross section is shown in Figure 7 with a harmonic potential of the same frequency and equilibrium position (dashed line). Despite the shape of this potential, the computed spectrum indicates that the energy levels in this mode are only slightly anharmonic. This suggests that the appearance in a spectrum of evenly spaced lines does not necessarily correspond to a harmonic potential in that vibration.

The relative intensities displayed in the DPC-4 spectrum are also well reproduced by the computed spectrum. In fitting the potential to the spectrum, more care was taken to fit the positions of the eigenvalues to the observed energy spacings, with the equilibrium position of the excited state determined automatically by the parameters used. In other words, once the computed energy levels were fit to the observed spectrum, no further adjustments were made in the parameters to adjust the equilibrium displacements between the two surfaces and tune the relative intensities of the peaks. As a result, the minimum on the DPC-4 empirical surface occurs at $\alpha_{\text{min}} = 133.4^\circ$ and $\phi_{\text{min}} = 25.7^\circ$ (compared to the values 136.5° and $\sim 21^\circ$, respectively, for the S_0 state). The resulting displacement for ϕ , $\sim 4.7^\circ$, is in fairly good agreement with the estimated value of $5\text{--}6^\circ$ found above, while the displacement in α , 3.1° , is a bit less than the estimated displacement ($\sim 4^\circ$) from the experimental spectrum. This means that the peaks in the various bend progressions will tend to increase in intensity faster in the experimental spectrum than in the simulated spectrum, which is indeed the case. Using eq 3.12 to assign α_{eq} , which serves to set the probable value of α_{min} , provides a consistent definition that can be used for all of the molecules studied; however, substituting a smaller value of α_{eq} in the bend potential *does* have the effect of correcting the small discrepancies between the calculated and observed relative intensities.

The empirical surface used in computing the spectrum is shown in Figure 8 as a contour plot with different contours spaced by 250 cm^{-1} above the potential minimum. This picture suggests that the barrier to the perpendicular phenyl ring twist configuration in DPC-4 is about 1500 cm^{-1} . Also shown in Figure 8 are a few snapshots from the dynamics of the Franck–Condon wave packet on that surface spanning $\sim 220 \text{ fs}$. Although such a wave packet could be created in the laboratory only by using an infinitely short laser pulse, its movement is indicative of the dynamical behavior of the molecule on the excited state.⁵⁵ Mathematically, its motion

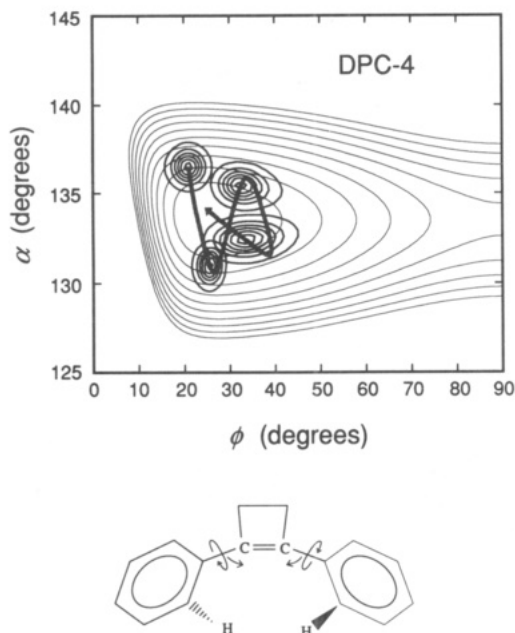


Figure 8. Portion of the potential surface for S_1 DPC-4 in the α and ϕ coordinates. The minimum on this surface occurs for $\alpha_{\min} = 133.4^\circ$ and $\phi_{\min} = 25.7^\circ$, and the contours are spaced evenly by 500 cm^{-1} with the potential minimum representing zero energy. From this picture, the barrier to rotation of the phenyl rings through a configuration roughly perpendicular to the cyclobutene ring is $<3000 \text{ cm}^{-1}$. Also pictured are snapshots depicting the initial dynamics of the Franck-Condon wave packet on the DPC-4 surface. Its origin, which corresponds to the equilibrium geometry of the S_0 surface ($\alpha = 136.5^\circ$, $\phi \approx 21^\circ$) is at the upper left. The initial motion is to smaller bond angles, α , and to larger twist angles, ϕ , as is illustrated in the representation of the molecule below the potential.

is also important in the determination of the spectrum through eq 3.19. Once the molecule has been promoted to the S_1 state, its motion immediately takes it to a smaller bond angle and larger phenyl twist angle. Since most of the wave packet is lower in energy than the $\sim 1500 \text{ cm}^{-1}$ barrier at $\phi = 90^\circ$ (this is actually a saddle point on the surface), it will continue to oscillate around the potential well indefinitely. It should be noted that the presence of the C-C bonding interaction in the empirical potential has essentially no effect on the shape of the potential within the pictured region and the C_2-C_2' distance is $\sim 3.2 \text{ \AA}$ at the potential minimum. These results are consistent with the observation that DPC-4 does not form the photocyclization product upon excitation.⁴

It should be emphasized that the approach used here to fit the DPC-4 spectrum is a very useful one for the treatment of a variety of different molecules, including the diphenylcycloalkenes and *cis*-stilbene, in that the model surface provides flexibility and a certain degree of predictive ability. If one were simply to use a model potential consisting of harmonic oscillators with a few anharmonic terms added on, one would be able to generate a computed spectrum that matches the experimental DPC-4 spectrum exactly (given enough time), even without specifying the vibrations involved. However, such a model would apply only to DPC-4 and there would be no practical way to extend the potential parameters to DPC-5 and DPC-6, nor would there be any appropriate way to check the effect of isotopic substitution on the frequencies. The fact that the empirical potential of the present study reproduces isotope shifts as well as equilibrium displacements between the two states is confirmation that it provides a good qualitative representation of the S_1 surface of DPC-4 in the α and ϕ coordinates. The fact that it is constructed from the additive combination of several completely general forces means that it can be extended naturally to study the excited-state dynamics of DPC-5 and DPC-6 as well.

B. Excited-State Dynamics of DPC-5 and DPC-6. Using the potential parameters k_a , V_2 , and V_4 found in the previous section,

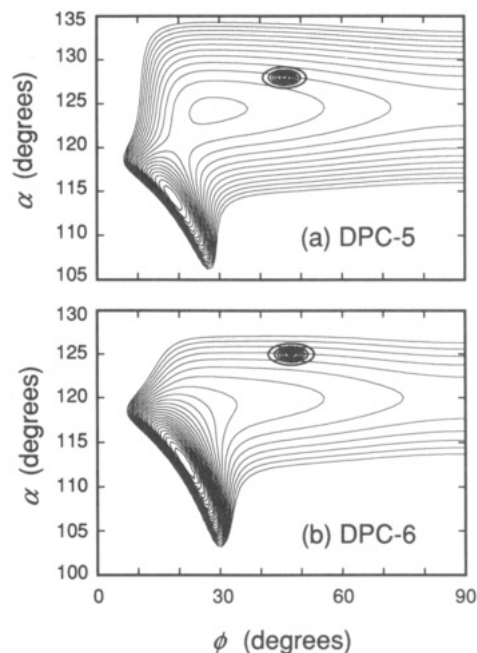


Figure 9. Simulated potential surfaces for (a) DPC-5 and (b) DPC-6 using the generalized force parameters from DPC-4. The contours are drawn at 1000-cm^{-1} intervals starting at the absolute minimum in the potential (lower left for both molecules) and are drawn only for the lowest 25000 cm^{-1} . For DPC-5, the surface contains two minima, corresponding to DPC-5 and the DHP analogue for DPC-5, separated by a barrier from the DPC-5 side of $\sim 800 \text{ cm}^{-1}$. For DPC-6, there is a single minimum that corresponds to the DHP analogue for DPC-6. The position of the Franck-Condon wave packet is pictured for both molecules—initial motion on both surfaces will be down and to the left, toward the DHP minima. Note that in the DPC-6 case, the initial wave packet is entirely above the barrier to rotation through a perpendicular configuration of the phenyl rings (relative to the cycloalkenyl ring), while most of the DPC-5 wave packet is below this energy barrier.

empirical surfaces for DPC-5 and DPC-6 can now be constructed. The only adjustments required are (i) to assign a new value for α_{eq} according to eq 3.12 by using the γ angles appropriate for DPC-5 and DPC-6, respectively, and (ii) to incorporate the new positions of the nearest cycloalkenyl ring H atoms into the V_{HH} potential. The implicit assumption is made that these molecules are similar enough to use the same conjugative and bending forces for all three. While this is probably reasonable for qualitative purposes, some changes should be expected as one goes from DPC-4 to DPC-5 and DPC-6 because these forces will depend in part on the electronic environment of the ethylenic carbons, C_e and $C_{e'}$. This environment changes as the cycloalkenyl ring gets larger and the bond angle, α , gets smaller. Once again, the ethylenic torsion angle, θ , is held fixed, although for DPC-5 and DPC-6 it is likely to be more flexible than for DPC-4.

The surfaces that result from applying the DPC-4 parameters to DPC-5 and DPC-6 are shown in Figure 9 along with the Franck-Condon wave packet. Several major qualitative differences are evident. Both of these molecules allow the two phenyl rings to come close enough to one another in the proper orientation to form DHP-like products. For DPC-5 there are actually separate minima on the surface for DPC-5 and its photocyclization product, which are separated by a barrier of $\sim 800 \text{ cm}^{-1}$ (2.3 kcal/mol) on the DPC-5 side. The second minimum, at $\alpha = 113.5^\circ$ and $\phi = 18.5^\circ$, corresponds to a C_2-C_2' distance of 1.56 \AA , which is close to the equilibrium separation used in the V_{CC} potential, indicating that the C-C bond was formed. In DPC-6, there is only one minimum, occurring at $\alpha = 112.5^\circ$ and $\phi = 21.5^\circ$, and this corresponds to a C_2-C_2' separation of 1.53 \AA —exactly the equilibrium bond distance of the V_{CC} potential.

These features are in accord with experimental observation. No emission is observed for isolated DPC-5 or DPC-6, meaning that these molecules decay quickly by radiationless processes that include the formation of the photocyclization product.^{16,58} A

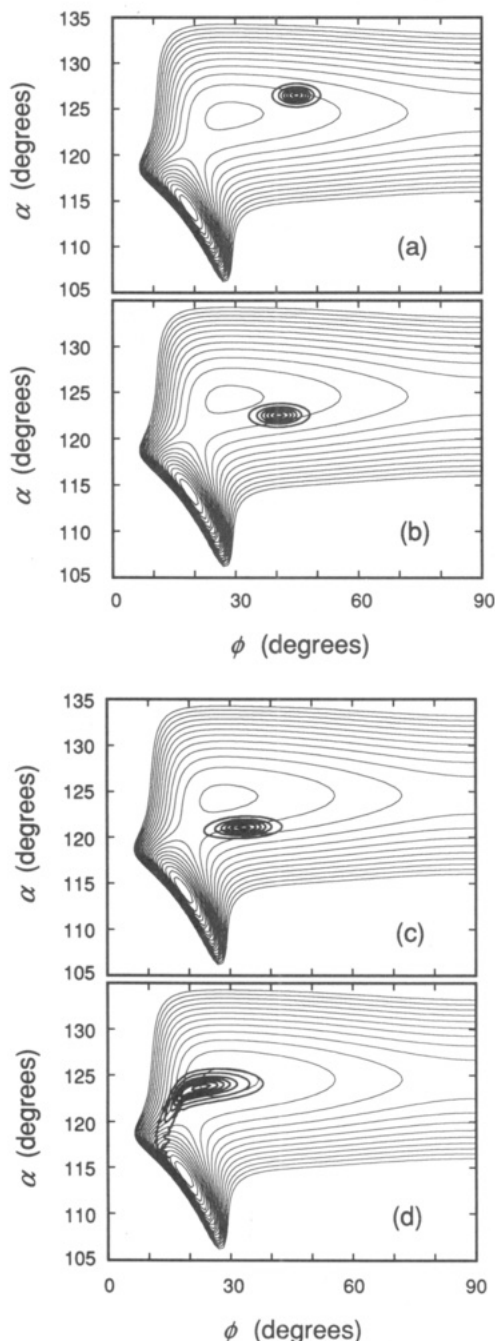


Figure 10. Snapshots from the early dynamics of the Franck-Condon wave packet on the DPC-5 empirical potential surface. The total time span of the dynamics shown is about 220 fs. The wave packet originates at the position indicated in Figure 9a, and then moves toward the lower left corner of the potential where the photocyclization product (DHP analogue) is formed. Since the wave packet is moving parallel to the gap leading to DHP in this case, only a small portion "leaks" over into the DHP region of the potential (d).

barrier of DHP formation in DPC-5 of ~ 2.6 kcal/mol has been inferred from experimental observations¹⁶ and the estimated quantum yield of this product is $\sim 50\%$ (see Table I). The barrier of 2.3 kcal/mol found for the empirical surface of DPC-5 is in good agreement with the inferred value. DPC-6, on the other hand, is believed to have no barrier to photocyclization,⁴ and the quantum yield of the DHP-like product, while not measured, is reported to be high.⁵⁸ Again, the surface constructed for DPC-6 reflects these properties.

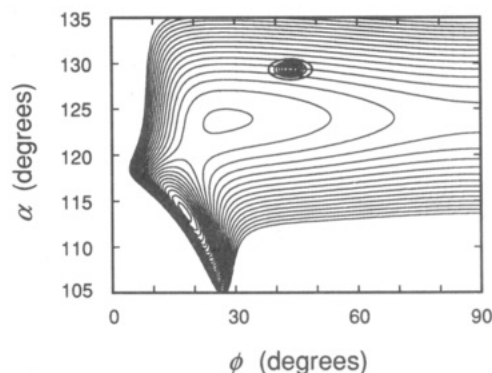


Figure 11. Simulated potential surface for *cis*-stilbene, drawn at the calculated ground-state equilibrium angle, $\theta = 9^\circ$. Potential contours are drawn at 1000-cm^{-1} intervals beginning at the global minimum of the surface (at lower left) and are drawn only for the lowest $25\,000\text{ cm}^{-1}$. Like DPC-5 (Figure 9a), the potential contains two minima representing *cis*-stilbene (central) and DHP (lower left), which are separated by an energy barrier of about 535 cm^{-1} . The Franck-Condon wave packet is pictured at the upper right. As for DPC-5 and DPC-6, the initial motion of the wave packet will be down and to the left, toward the DHP region of the potential.

For both DPC-5 and DPC-6, the equilibrium twist angle is smaller than in the ground electronic state. This means that the initial dynamics of both molecules is toward smaller bend and twist angles and is favorable for forming the photocyclization product rapidly. Several snapshots from the dynamics of the Franck-Condon wave packet on the DPC-5 surface are shown in Figure 10. In particular, note that when the wave packet first traverses the DPC-5 well, it encounters the saddle point connecting the two products, and a small piece of it crosses into the "DHP" region of the potential. It can be seen that the wave packet begins with more than enough energy to cross the barrier to the DHP region, but it must be moving in the proper direction when it reaches the barrier for any appreciable piece to leak over into the other well. Although one cannot draw quantitative conclusions from the use of this potential, the qualitative implications of the dynamics are clear; the initial motion of the molecule on the excited-state surface leads to configurations that favor the formation of the photocyclization product.

The fact that the phenyl twist angle decreases in DPC-5 and DPC-6 upon excitation to S_1 is notably different from the observed behavior in DPC-4, where ϕ increases. This seeming contradiction is a result of the delicate balance of forces that determine the equilibrium twist geometries for both the ground and excited states. In the case of DPC-4, the decrease in the bond angle, α , brings the H_2 and $H_{2'}$ atoms closer together, and their repulsive interaction overbalances the stronger conjugative force in the excited state and causes the phenyl rings to twist farther away from the planar configuration. For DPC-5 and DPC-6, the initial twist angle is much larger than for DPC-4 (46° for DPC-5 and 47° for DPC-6) due to the smaller equilibrium value of α on the ground-state surface. When these molecules are promoted to the excited state, the stronger conjugative force then dominates the change in the equilibrium twist angle and ϕ decreases. Interestingly, the attractive interaction between the C_2 and $C_{2'}$ atoms plays no role whatsoever in determining the change in ϕ_{\min} from S_0 to S_1 —the same results are obtained when the C-C bonding interaction is omitted from the empirical potential.

C. Implications for Stilbene Dynamics. Although it is clear that motion in the ethylenic torsion angle is important to any consideration of the dynamics on the excited singlet surface of stilbene, the parameters used in the diphenylcycloalkene potential surfaces for constant θ can be applied to *cis*-stilbene to learn more about its S_1 force field. The result of this application is shown in Figure 11, where the potential in the α and ϕ coordinates is shown for the theoretically predicted⁵⁹ ground-state equilibrium

(58) Ito, K.; Tazuke, S. *Symposium of Photochemistry 1989: Proceedings, Miyazaki, Japan 1989*, 433-434. The quantum yield for DHP formation is not reported in this work, but it is shown that DHP formation is the major photochemical channel.

(59) Kao, J.; Allinger, N. L. *J. Am. Chem. Soc.* **1977**, *99*, 975. Kao, J. *J. Am. Chem. Soc.* **1987**, *109*, 3817.

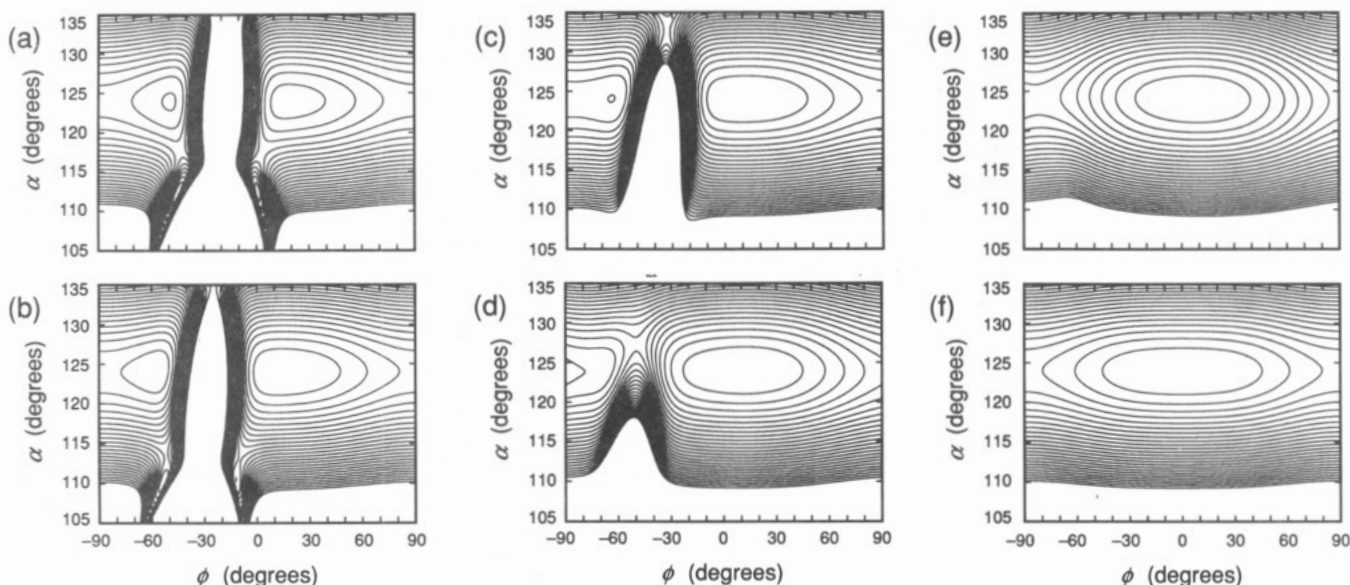


Figure 12. Several cross sections of the stilbene potential surface in the α and ϕ coordinates corresponding to $\theta =$ (a) 30° , (b) 45° , (c) 60° , (d) 90° , (e) 120° , and (f) 180° . Potential contours are drawn at 1000-cm^{-1} intervals beginning with the global minimum on the surface. Regions in which no contours appear are at higher energies than the highest contour ($25\,000\text{ cm}^{-1}$). As the ethylenic torsion angle changes from a *cis*-stilbene configuration ($\theta = 9^\circ$) to a *trans*-stilbene configuration ($\theta = 180^\circ$), the topology of the surface changes radically, indicating the importance of the interphenyl ring forces in promoting the differences between *cis*- and *trans*-stilbene.

value, $\theta = 9^\circ$, and the excited-state theoretical value, $\alpha_{\text{eq}} = 123.9^\circ$.¹⁵ As in Figure 9, the Franck-Condon region is indicated by the presence of the initial wave packet on the *cis*-stilbene surface.

Given the similarity in the geometries of the two molecules, it is no surprise that this surface is very similar to that found for DPC-5 (Figure 9a). Like DPC-5, there are two minima, one corresponding to *cis*-stilbene at $(\alpha, \phi) = (123.9^\circ, 26.8^\circ)$ and the other corresponding to DHP, at $(\alpha, \phi) = (113.4^\circ, 17.8^\circ)$, which are separated by a barrier of 535 cm^{-1} (1.5 kcal/mol) on the stilbene side. Once again, the initial dynamics should display motion toward smaller α and smaller ϕ and should closely approach the DHP region of the potential, suggesting that the photocyclization reaction is an important channel in the early dynamics of the *cis*-stilbene photoisomerization reaction. As in DPC-5, the initial wave packet mostly occurs at energies above the barrier to DHP formation but must approach the saddle point at $(\alpha, \phi) = (120.4^\circ, 19.4^\circ)$ from the proper direction for any appreciable probability density to cross into the DHP region.

Though there has been no attempt to model the potential along the ethylenic torsion coordinate, it is nevertheless useful to look at cross sections of the bend/twist potential for different values of θ . Several of these cross sections corresponding to $\theta = 30^\circ$, 45° , 60° , 90° , 120° , and 180° (*trans*-stilbene) are displayed in Figure 12. Unlike the earlier plots, ϕ is now shown over the range -90° to 90° , so that the effects of *cis*-*trans* isomerization on the bend/twist potential can be seen fully. Due to the symmetry of the molecule, the potential in this range is identical with that in the range 90 – 270° .

The stilbene bend/twist potential undergoes an interesting evolution as θ increases. At $\theta = 30^\circ$, the potential still displays a well corresponding to DHP, but the depth of this well has decreased from 9900 cm^{-1} for $\theta = 9^\circ$ to 5500 cm^{-1} , meaning that the C–C bond weakens with increasing θ , as expected. By the time θ reaches 45° , the DHP region has grown considerably smaller and less stable with a depth $<1000\text{ cm}^{-1}$. When $\theta = 60^\circ$, the DHP region no longer exists—the phenyl rings are too far apart for the bonding interaction to occur. A second saddle point has also become visible at the top of the contour plot, and the minima in the surface have shifted over so that the more stable well is near $\phi = 10^\circ$. As the molecule approaches a perpendicular configuration ($\theta = 90^\circ$), the weaker of the two minima has all but disappeared with the other well more stable by $\sim 5000\text{ cm}^{-1}$. This geometry corresponds to that of the postulated intermediate,

¹p, in stilbene's *cis*-*trans* isomerization (see Figure 1).²² At $\theta = 120^\circ$, there is a single minimum on the surface near $\phi = 0^\circ$, and the barrier to free rotation of the phenyl rings is $\sim 6500\text{ cm}^{-1}$. This barrier continues to decrease as θ increases until it reaches a value of 3200 cm^{-1} in the *trans* configuration ($\theta = 180^\circ$). Since this represents both of the phenyl rings rotating, the barrier for a single ring to freely rotate is actually $\sim 1600\text{ cm}^{-1}$.

The results for the *trans* configuration of stilbene can be compared with various experimental observations. Park and Waldeck have recently estimated the barrier to free rotation of the phenyl rings in *trans*-stilbene to be $\sim 750\text{ cm}^{-1}$.³¹ This is about half the value derived from the current empirical potential surface, which arises almost entirely from the value of V_2 . Unfortunately, using smaller values of V_2 , particularly $V_2 = 1500\text{ cm}^{-1}$ (again accounting for the factor of having two phenyl rings), leads to an unsatisfactory fit of the DPC-4 spectrum. Such values cause the progressions in the phenyl twist to be too anharmonic and also decrease the displacement between the ground- and excited-state surfaces, further increasing the disparity between the calculated and observed relative intensity patterns. Nevertheless, the discrepancies between the present results and those of Park and Waldeck require further investigation.

V. Summary

The results of this paper may be summarized as follows:

(i) The spectroscopy and photophysics of a series of *cis*-stilbene prototype molecules, the 1,2-diphenylcycloalkenes, have been investigated experimentally. Of this group, 1,2-diphenylcyclopentene (DPC-5) is found to have properties most similar to *cis*-stilbene; however, 1,2-diphenylcyclobutene (DPC-4) provides even more valuable information about the low-frequency motions in this series of molecules because it emits as a free molecule.

(ii) The low-energy portion of the high-resolution fluorescence excitation spectrum of DPC-4 has been attributed to activity in three vibrations of frequency: 46 , 70.6 , and 151.4 cm^{-1} . These vibrations are identified as the out-of-plane bend, the symmetric phenyl twist, and the symmetric bend, respectively. A theoretical analysis of the spectrum reproduces the observed isotope shift for these vibrations, providing confirmation of the assignment.

(iii) An empirical potential surface has been constructed for the S_1 state of DPC-4 that reproduces both the observed line positions and the relative intensities for the symmetric bend and phenyl twist vibrations. This surface models several generalized forces in the molecule, including the bend potential, the π -system

conjugative force, which favors planarity, various nonbonded H-H repulsive interactions, and the C₂-C₂ attractive (bonding) interaction.

(iv) The DPC-4 empirical surface indicates that upon excitation, the symmetric bend angle decreases by 3–4° and the phenyl twist angle increases by 4–5°. The large equilibrium value of α , however, prevents the molecule from exploring configurations that lead to photocyclization.

(v) The parameters used to represent the generalized forces of S₁ DPC-4 have been adapted to the geometries of DPC-5 and DPC-6 to produce excited-state potential surfaces for these molecules. Unlike DPC-4, the phenyl twist angle in these molecules decreases upon excitation, leading to structural configurations that favor photocyclization. In DPC-5, a 2.3 kcal/mol barrier to the formation of the DHP analog is found, while in DPC-6, the path to photocyclization proceeds with no barrier.

(vi) Application of the DPC-4 generalized force parameters to *cis*-stilbene leads to a potential surface with topology very similar to that of DPC-5. In particular, the small barrier to DHP formation of 1.5 kcal/mol on this surface agrees well with the thermochemical studies of Fischer, Muszkat, and co-workers,¹⁶ who inferred a barrier of 1.2 kcal/mol from their observations.

(vii) The dynamics of the Franck-Condon wave packet on the DPC-5 S₁ surface (Figure 10) and the similarities between DPC-5 and *cis*-stilbene suggest that initial motion of *cis*-stilbene upon photoexcitation is along a coordinate that favors photocyclization. Moreover, the time scale of *cis*-stilbene nonradiative decay in the gas phase, 320 fs,⁶⁰ is comparable to the time it takes for the Franck-Condon wave packet to cross the well in DPC-5 and enter the region corresponding to photocyclization product, which is ~220 fs. Thus, there is strong evidence to suggest that the photocyclization channel may play a crucial role in the excited-state dynamics of *cis*-stilbene during photoisomerization. Unlike DPC-5, however, concurrent motion along the ethylenic torsion in *cis*-stilbene serves to limit the final quantum yield of DHP.

Although the calculated height of the barrier to DHP formation on the excited state, 1.5 kcal/mol, is remarkably consistent with the experimental value of 1.2 kcal/mol,¹⁶ it should be noted that the error in both of these determinations is likely to be great and that the agreement between them may be largely coincidental. A more reasonable comparison to make involves the barriers to photocyclization on the DPC-5 S₁ state because the empirical potential is more tailored to the diphenylcycloalkene structure. In this case, the excellent agreement between the experimental value¹⁶ of 2.6 kcal/mol and the calculated value of 2.3 kcal/mol indicates that the surface provides a good representation of the excited-state potential. Many approximations have gone into the construction of the empirical surface; however, it should still provide a *qualitatively* accurate picture for the excited state of

cis-stilbene. The qualitative prediction of a small versus a large barrier on the surface is important because this affects the absolute branching ratio between *cis*-trans and *cis*-DHP photoisomerization reactions in the free molecule. In solution, however, solvent stabilization effects can lead to overemphasis of one or the other product.

Since the oscillator strength for DHP is about half that of *cis*-stilbene,¹⁶ the DHP S₁ state will be less stabilized by solvation than *cis*-stilbene. One consequence of differential solvation of the two isomers is that the barrier to isomerization is likely to be solvent dependent. Similar solvent dependence of the barrier has been observed by a number of workers for the isomerization of *trans*-stilbene, where the barrier in alcohols is 2.5–3.0 kcal/mol lower than in hydrocarbons.¹ This observation is significant because recent studies by Hochstrasser² and Fleming³ and their co-workers have investigated the viscosity effect on the *cis*-stilbene isomerization rate by measuring the decay of the *cis*-stilbene S₁ state in alcohol and hydrocarbon solvents of different viscosity. There is a strong possibility that changing the solvent changes not only the viscosity of the medium but also the barrier for DHP formation and hence the branching ratio between *cis*-trans and *cis*-DHP isomerization channels. Since accurate measurements of the quantum yield for DHP formation have been made only in a methylcyclohexane/2-methylpentane solvent mixture, it is imprudent to assume that the contribution of the DHP isomerization channel to the *cis*-stilbene decay is constant and negligible.

The theoretical results obtained here depend on an extrapolation of the DPC-4 excited-state surface to other molecules that, though similar to DPC-4, are nevertheless different. Thus, the generally good agreement with various *quantitative* measurements, while gratifying, may be largely fortuitous. The empirical potential presented here represents an effort to learn about the *qualitative* dynamics on the excited state of these molecules, and, in this respect, it is quite useful. Further work on these systems will be concerned with trying to make the empirical surface more quantitatively accurate and extending the dynamics studies to include motion in the ethylenic torsion. As more is learned about the general forces that shape the structure and dynamical properties of molecules such as *cis*-stilbene, the ability to predict the structural changes and low-frequency dynamics that accompany a much wider variety of photochemical processes will be greatly enhanced.

Acknowledgment. J.H.F. thanks the Institute for Molecular Science in Okazaki for the warm hospitality extended during two visits in 1990 and the Research Advisory Board at the University of Nevada for funding one of those visits. Acknowledgment is made to the donors of the Petroleum Research Fund, administered by the American Chemical Society, for the support of this work (J.H.F.).

Registry No. DPC-4, 3306-02-3; DPC-5, 1485-98-9; DPC-6, 41317-87-7; *cis*-stilbene, 645-49-8.

(60) Greene, B. I.; Farrow, R. C. *J. Chem. Phys.* **1983**, *78*, 3336.